PHILOSOPHICAL TRANSACTIONS OF THE ROYAL SOCIETY A MATHEMATICAL, PHYSICAL & ENGINEERING SCIENCES

Solution of the Tidal Equations for the M$_{2}$ and S $_{2}$ Tides in the World Oceans from a Knowledge of the Tidal Potential Alone

Y. Accad and C. L. Pekeris

Phil. Trans. R. Soc. Lond. A 1978 **290**, 235-266
doi: 10.1098/rsta.1978.0083

SOLUTION OF THE TIDAL EQUATIONS FOR THE M_2 AND S_2 TIDES IN THE WORLD OCEANS FROM A KNOWLEDGE OF THE TIDAL POTENTIAL ALONE

By Y. Accad and C. L. Pekeris

Department of Applied Mathematics, The Weizmann Institute, Rehovot, Israel

(*Communicated by Sir Harold Jeffreys, F.R.S. – Received* 16 *February* 1978)

CONTENTS

Laplace's tidal equations are solved for the M_2 and S_2 tides in the world oceans on the basis of a knowledge of the tidal potential alone. Tidal dissipation was taken to be limited to the coastline, where a fraction of the tidal energy incident on the coast was assumed to be absorbed. The coast was assumed to be either vertical or to have a sloping shelf, the latter model yielding results in better agreement with observations. The main purpose of this investigation was to determine the effects of tidal self-attraction and of tidal loading. A fast iterative method was developed by which these secondary effects could be evaluated. The resulting change is of the order of 10%, and somewhat improves the agreement between the theoretical and observed tides. Tidal dissipation from the M_2 and S_2 tides totals 3.1×10^{19} erg/s. The total retarding couple exerted by the M_2 and S_2 tides on the Earth comes out at 4.2×10^{23} dyn cm, yielding a deceleration of the Earth's rotation from these sources of $1080''/cy^2$. The theoretical tidal values were

Vol. 290. A. 1368 19 [Published 28 November 1978

compared with observations on the northeastern and western coasts of the Pacific, on the western coast of the Atlantic, on New Zealand, and on islands. The theoretical tidal phases are generally within one hour of the observed values; the amplitudes are in reasonable agreement with observations except in zones where there is amplification by the fiord effect. A solution obtained for a 'smoothed' coastline showed little change.

Note on units.

1 erg = 10^{-7} J.
1 dyn = 10^{-5} N.
In this paper the symbol cy is used for century.

1. Introduction

The question whether a knowledge of the tidal potential alone suffices to determine the tides in the world oceans was posed over 200 years ago by Laplace (1775) when he derived the tidal equations that bear his name. From the point of view of applied mathematics the goal is tantalizing: with an input of only a single number, namely the known amplitude of the harmonic component of the tidal potential, we wish to determine the height and phase of the harmonic in the tide at every coastal station and at every point in the open ocean. There are known some 1300 'representative' tidal stations located on the coasts and on islands, in addition to about a dozen tidal stations in the open ocean where the tide was measured by recording the pressure with an instrument placed on the bottom. At each station the amplitude and phase of the tidal harmonic were determined. Further data are forthcoming from observations of the gravity tide (Harrison *et al.* 1963; Kuo & Jachens 1977).

The feasibility of this project, including some preliminary results, was reported by Pekeris & Dishon at the I.U.G.G. meeting in Helsinki in 1960. It was already known then that this task would be much more difficult than the companion project of using the observed tides on islands and at coastal stations to interpolate for the tide in the open ocean with the aid of Laplace's tidal equations (Dietrich 1944; Bogdanov & Magarik 1967; Tiron, Sergeev & Michurin 1967). The simplification gained in the boundary conditions and from dispensing with the solution of Laplace's tidal equations at the coastal stations is marred, however, by the impossibility of satisfying the equation of continuity there. Thus in Hendershott & Munk's solution for the M_2 tide (1970), the *average* sea-level fluctuates with an amplitude of 6.8 cm (Farrell 1972). An amplitude of 6.8 cm in the unwanted zero-order harmonic ζ_0 of the tide ζ amounts to some 25 % of the global average amplitude of the tide $\langle|\zeta|\rangle$, which is around 25 cm (see below; in our solutions, to be given below, ζ_0 is only of the order of a millimetre).

The recognition of the significance of tidal friction as one of the controlling factors in the dynamics of oceanic tides was forced upon us by the work reported in our first paper (Pekeris & Accad 1969; this paper will be referred to as I). Ignoring friction, as we attempted to do in the first instance, resulted in the following malignancies: (1) abnormally large tidal amplitudes; (2) sensitivity of the solution to small changes in the boundaries; and (3) slowness of numerical convergence as the computational grid-size was reduced. When friction was introduced, these symptoms disappeared. In this work, dissipation (of the albedo type) is introduced *ab initio*.

The main theme of our present work is the treatment of the effect on the tides of the elastic yielding of the Earth due to tidal loading and to the self-attraction of the tides. The significance of the effects of tidal loading and of self-attraction has been stressed recently by Farrell (1973) and Hendershott (1972). We have developed an iterative method of solution by which these secondary effects can be evaluated, and the result will be shown for the M_2 tide and the S_2 tide.

The effect of tidal loading and of self-attraction introduces a correction in the tides, as well as in the gravity tide, of the order of 10 %. To the extent that this residual effect can be determined with reasonable accuracy it takes on a geophysical significance of a nature which at first seems surprising. Because the period of the tides is some fourteen times longer than the lowest period of free oscillations of around 54 min, the dynamic response of the Earth to tidal loading and self-attraction depends on the deep structure of the Earth down to the interior of the liquid core. Thus, for a uniformly stable core-model there exist, in addition to the normal free oscillations with lowest period of 53.7 min, an infinite number of 'core oscillations' (Pekeris & Accad 1972, figs 6 and 8) whose free periods, for $n = 2$, are (in hours) 7.4, 11.7, 16.0, 20.3, 24.3, ... At these free periods the Love numbers become infinitely large. An earthquake cannot excite them because the crust, indeed the whole mantle, is a nodal zone for the core oscillations. On the other hand, the tidal potential is of order unity in the core, and, furthermore, it is not a transient phenomenon, but acts permanently. Tidal observations are, therefore, potentially a source of information on the existence or non-existence of core oscillations.

The topography of the ocean model adopted is shown in figure 1. The coastline is built up of arcs of longitude and latitude of length 2° in Mercator coordinates. Tidal dissipation is assumed to occur only at the coast, where a fraction of the tidal energy incident on the coast is assumed to be absorbed either according to the Proudman model shown in figure 2, or according to the sloping-shelf model shown in figure 3. Figures 4 and 5 give the tidal solution for the two models when the secondary effects of tidal loading and of tidal self-attraction are neglected, the sloping shelf solution shown in figure 5 appearing to be the more satisfactory one.

The contribution to the tide arising from the secondary effects of tidal loading and tidal self-attraction represented by ζ is shown, in the first approximation, in figure 6, where it is seen to be comparable in magnitude to the effective equilibrium tide $(1 + k_2 - h_2)\,\bar{\zeta}$. One notes the similarity between the ζ-map in figure 6 and the tidal map in figure 5, and this feature is taken advantage of in the representation (19) for the formulation of an iteration procedure. The rapidity of this K-iteration method is illustrated in table 2. The final solution with the secondary effects included is shown in figures 7 and 8, the latter conforming somewhat better with observations.

A detail of figure 8 is shown in figure 9, giving a comparison between theoretical and observed tidal values in the region of the northeast Pacific amphidrome discovered by Irish, Munk & Snodgrass (1971).

Further comparisons between theoretical and observed tidal values are shown in figures 10, 11, 12, and 14 for the northeastern Pacific coast, the western Atlantic coast, the western Pacific coast, and New Zealand respectively. Island stations are treated in table 3.

We found that the inclusion of the secondary effects of self-attraction and of tidal loading improved the theoretical solution somewhat, when judged by the degree of agreement between the observed and the theoretical M_2 tides.

We have evaluated the couple N exerted by the tide-producing body on the Earth, as well as the tidal dissipation D. The retarding couple N is given by the integral (24) taken over the *surface* of the oceans, whereas the dissipation D is represented by the *line-integrals* (27) and (28) taken along the coastline. It is seen from table 5 that the ratios (D/N) come out close to the value of 7.3×10^{-5} s^{-1} of the speed of rotation of the Earth, indicating that most of the tidal dissipation energy is spent on slowing down the rotation of the Earth. The values of tidal dissipation and of the retarding torque on the Earth due to the M_2 and S_2 tides come out in line with accepted values.

The solution for the S_2 tide shown in figure 16 is similar in appearance to the solution for the M_2 tide shown in figure 8. Indeed, the ratio of the tidal dissipations for the M_2 and S_2 tides comes out

PHILOSOPHICAL TRANSACTIONS OF THE ROYAL SOCIETY A MATHEMATICAL, PHYSICAL & ENGINEERING SCIENCES

close to the square of the ratio of the amplitudes of the respective equilibrium tides (Jeffreys 1976, p. 319).

We have investigated the possible error stemming from the sharp corners introduced in the finite-difference scheme by approximating the 'continuous' coastline (marred, alas by fiords and bays) by arcs of longitude and latitude. An ocean-model with a smooth coastline was prepared, as detailed in appendix B. The tidal solutions yielded by the smooth model shown in figures 17 and 18 do not deviate appreciably from the corresponding solutions for the rough coastline given in figures 5 and 8, the solution for the smooth model being a shade less satisfactory.

2. Modification of the tidal potential due to tidal self-attraction and to tidal loading

Let Ω denote the gravitational potential, defined so that the force $\boldsymbol{F}$ per unit mass is given by

$$\boldsymbol{F} = -\operatorname{grad}\Omega. \tag{1}$$

With $\bar{\Omega}$ denoting the astronomical tidal potential, and $\bar{\zeta}$ denoting, in the standard notation (Lamb 1932, p. 332), the equilibrium tide, we have

$$\bar{\Omega} = -g\bar{\zeta}. \tag{2}$$

For the M_2 tide we have

$$\bar{\zeta} = 24.25\sin^2\theta e^{i(\sigma t+2\lambda)}\,\text{cm}, \tag{3}$$

where θ and λ denote colatitude and east longitude, and σ is the frequency of M_2. Let ζ denote the tidal elevation relative to the bottom. If ζ_s is the tidal elevation of the surface relative to the centre of the Earth, and ζ_b the tidal elevation of the bottom relative to the centre of the Earth, then

$$\zeta = \zeta_s - \zeta_b. \tag{4}$$

From this definition of ζ it follows that the equation of continuity retains the Laplacian form

$$\frac{\partial\zeta}{\partial t} = -\frac{1}{a\sin\theta}\left[\frac{\partial}{\partial\theta}(hu\sin\theta)+\frac{\partial}{\partial\lambda}(hv)\right], \tag{5}$$

where u and v denote the components of velocity (assumed uniform throughout the oceanic column), and $h(\theta,\lambda)$ is the variable depth of the ocean. In the presence of a bottom frictional force with components $F_{B\theta}$ and $F_{B\lambda}$, Laplace's tidal equations take the form

$$\frac{\partial u}{\partial t} - 2\omega v\cos\theta = -\frac{g}{a}\frac{\partial\zeta'}{\partial\theta}+\frac{1}{\rho h}F_{B\theta}, \tag{6}$$

$$\frac{\partial v}{\partial t} + 2\omega u\cos\theta = -\frac{g}{a\sin\theta}\frac{\partial\zeta'}{\partial\lambda}+\frac{1}{\rho h}F_{B\lambda}, \tag{7}$$

where ω is the speed of rotation of the Earth. In the original Laplace formulation (Lamb 1932, p. 332), ζ' stood for $(\zeta-\bar{\zeta})$, but this must now be modified to include (1) the effect of the elastic yielding of the Earth to the direct action of the astronomical tidal potential, (2) the effect of the elastic yielding of the Earth to the tidal loading, and (3) the self-attraction of the tides. If $-g\xi$ denotes the change in the gravitational potential due to effects (2) and (3), we have, by conventional theory,

$$\zeta' = \zeta-(1+k-h)\,\bar{\zeta}-\xi, \tag{8}$$

where k and h are Love numbers,

$$\zeta(\theta,\lambda) = \alpha \sum_n \frac{\epsilon'_n \zeta_n}{(2n+1)} = \frac{\alpha}{4\pi}\int_0^{2\pi} d\lambda' \int_0^{\pi} \sin\theta' \, d\theta' \zeta(\theta',\lambda') \sum_n \epsilon'_n P_n(\cos\theta'), \tag{9}$$

$$\epsilon'_n = 1 + k'_n - h'_n, \tag{10}$$

$$\alpha = 3\rho/\bar{\rho} = 0.56, \tag{11}$$

and the axis of the coordinate system (θ', λ') passes through the point (θ, λ).

Here k'_n and h'_n denote loading Love numbers, $\bar{\rho}$ the mean density of the Earth ($= 5.57$ g cm^{-3}), and ζ_n denotes the nth spherical harmonic component of the tide ζ:

$$\zeta = \sum_{n=1}^{\infty} \zeta_n. \tag{12}$$

In (12) we have omitted the term ζ_0, because it comes out to be only of the order of a millimetre for the two types of boundary conditions which we have used.

3. The topography of the ocean bottom

The ocean topography was based on the data published by Dishon & Heezen (1968), which contain about a million soundings. The average observed depth in a square of 1° in Mercator coordinates around a grid-point was taken as the initial value of the depth for that point. In this way the depth at about half the number of the grid points was determined. The depth at points on the coast was derived on the basis of the bottom slopes in the neighbouring oceanic points. There remained blank areas where the depth was interpolated, on the basis of the depth at the boundaries of the area, through the scheme:

$$h(i,j) = \tfrac{1}{4}[h(i-1,j) + h(i,j-1) + h(i+1,j) + h(i,j+1)]. \tag{13}$$

This procedure yielded a rough topography. These initial data were then subjected to a smoothing operation by taking for each point the weighted average depth of the neighbouring points according to the weighting scheme:

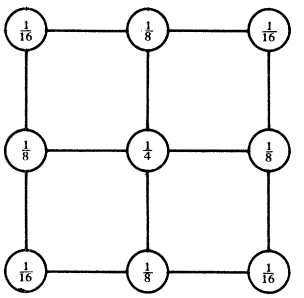

Five smoothing operations were applied for the basic 1° map.

Figure 1 shows the 1° map from which was derived the 2° map used in our present calculations. It gives the depth-contours in metres. Note that not only were such features as the English Channel not included, but even the Mediterranean Sea was eliminated. Any topographic feature whose dimensions were smaller than the grid-size of 2° had, of course, to be smoothed over. The representation in the model of shallow seas was particularly difficult. In contrast to I, where a lower limit to the depth of 1 km was imposed, the depth in the new ocean model was unrestricted.

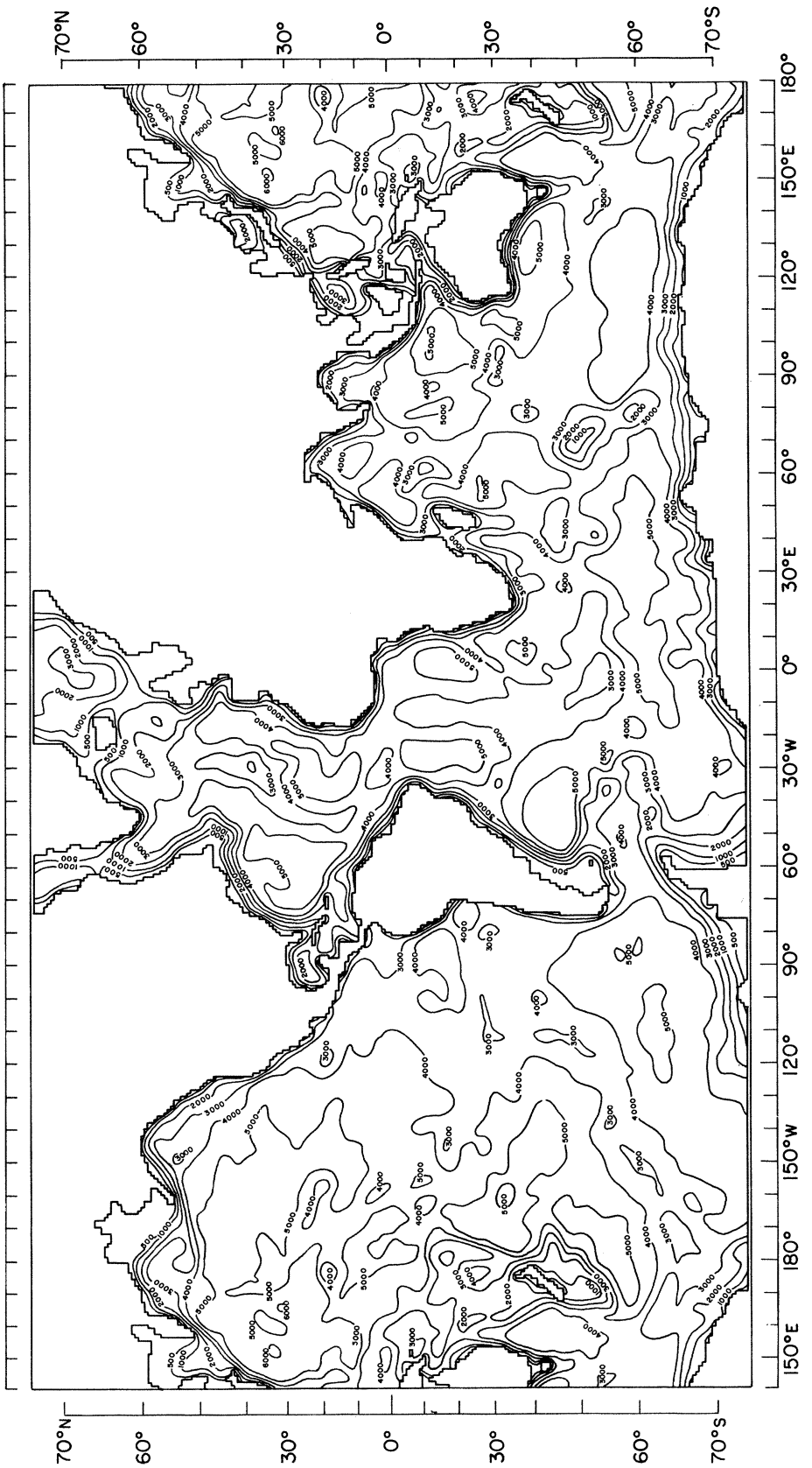

FIGURE 1. 1° map. Contour lines of depths of world oceans (in metres).

4. Tidal friction

In this work, bottom-friction was neglected and two models of the albedo-type dissipation were considered. The first model, designated as the Proudman model (Proudman 1941; see also Jeffreys 1968), is shown in figure 2. It is assumed that of the tidal energy which is incident on the

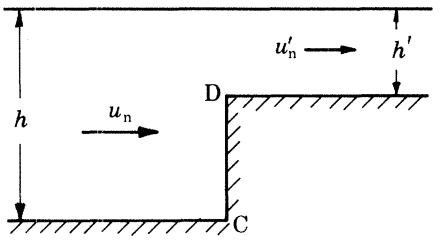

Figure 2. The Proudman model of coastal dissipation.

shore CD, the fraction contained in the upper layer of thickness h' is not reflected, but is lost on shore by tidal dissipation. Since for the progressive wave in the channel of depth h' we have

$$\sqrt{(gh')}\,\zeta = h'u'_n, \tag{14}$$

and since, by the equation of continuity,

$$h'u'_n = hu_n, \tag{15}$$

we get the Proudman relation between the component of velocity normal to the shore u_n and the tide ζ,

$$hu_n = \sqrt{(gh')}\,\zeta. \tag{16}$$

This was the boundary condition applied at the coastal grid-points.

In the second model we assume a sloping shelf starting at the boundary point C, as shown in figure 3.

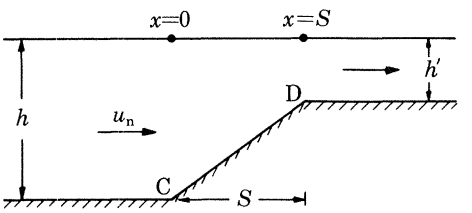

Figure 3. The sloping-shelf model of coastal dissipation.

Again, the tidal energy included in the shallow channel of depth h' is lost by dissipation. Here, too, u_n and ζ at the boundary point C are linearly related:

$$hu_n = \sqrt{(gh)}\,\{(1-R)/(1+R)\}\,\zeta, \tag{17}$$

where R is a complex reflexion coefficient which depends on the parameters S, h and h', as detailed in appendix A.

Figure 4 shows the solution for the M_2 tide when the Proudman boundary conditions were applied. The grid size was 2° in Mercator coordinates. We note that on the California coast there is a convergence of the cotidal lines, as if there were an amphidrome at a point inland not far from the coastline. Actually, Irish *et al.* (1971) have mapped out the so-called northeast Pacific amphidrome which is located some 1000 miles west of La Jolla. This amphidrome was identified

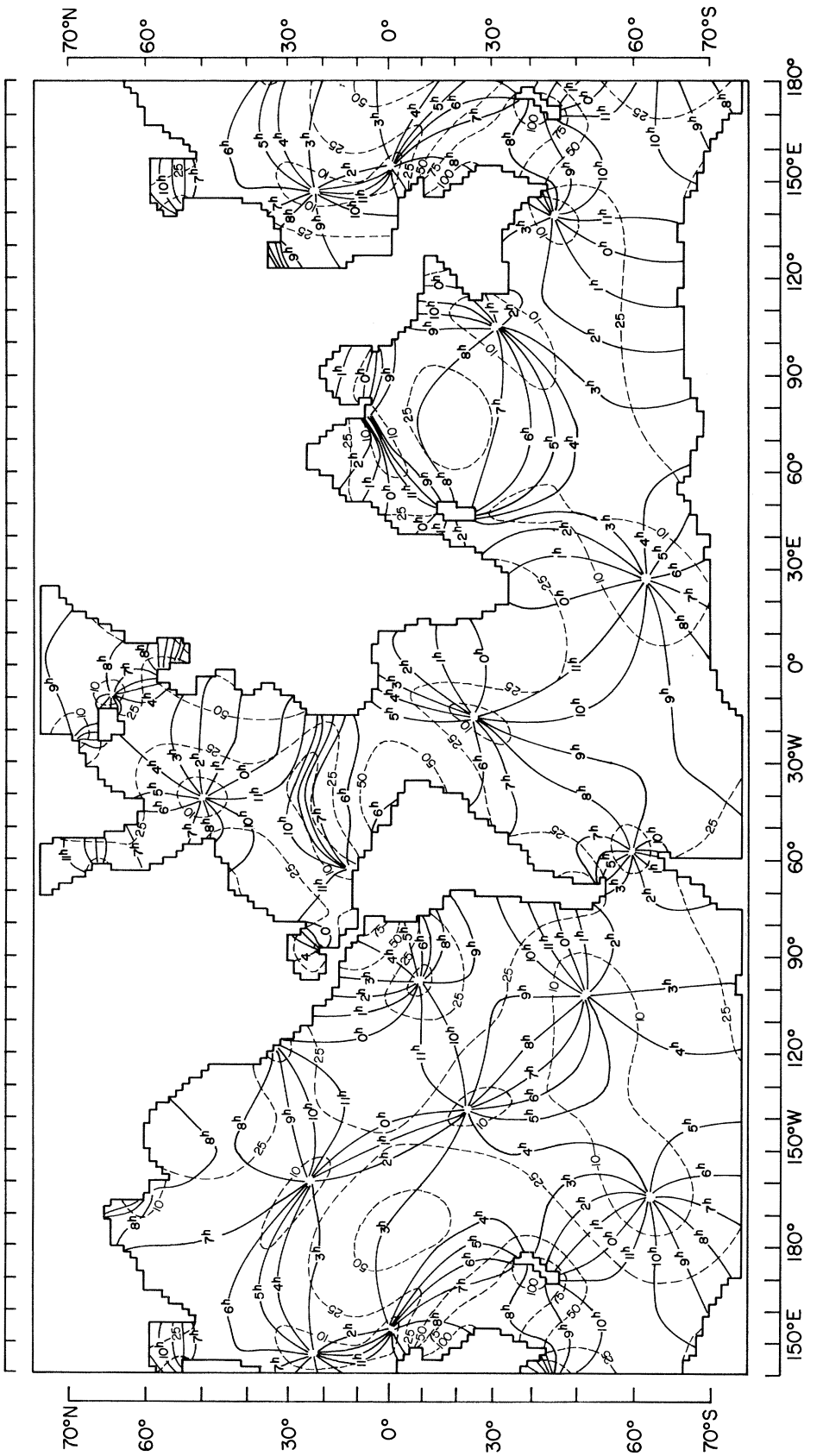

FIGURE 4. M_2 tide neglecting effects of self-attraction and of tidal loading. 2° grid, Proudman boundary condition, $h' = 25$ m. ——, Cotidal lines (Greenwich hours); – – –, corange lines (units: cm).

with the aid of six ocean-bottom stations, one of them being the Lamont station located some 100 miles from the coast, with recording done on the coast by cable connections. The Proudman map as it stands gives an M_2 tide on the California coast advancing southward, as against the observed tide which advances northward. This embarrassing feature was present also in our 1969 solution (Pekeris & Accad 1969) and did not pass unnoticed.

Leaving aside the California syndrome, one finds that generally the Proudman tidal map is advanced in phase by about $1\frac{1}{2}$ h relative to the observed values.

Figure 5 is the solution for the model with a sloping shelf. It does yield an amphidrome in the northeast Pacific, but, in this initial solution, the centre of the amphidrome is too close to shore. As a result, the theoretical tidal amplitudes on the coast near San Diego are around 25 cm, as against observed values of close to 50 cm. The phases are now about $\frac{1}{2}$ h less advanced than in the map with Proudman boundary conditions. This is still, on the average, about 1 h advanced relative to the observed values.

5. The treatment of the effects of tidal self-attraction and of tidal loading

As pointed out in §2, the effect of tidal self-attraction and of tidal loading is represented by a term $\hat{\zeta}$ which has to be added to the effective equilibrium tide $(1+k-h)\,\bar{\zeta}$. But, whereas the effective equilibrium tide is known in advance, the $\hat{\zeta}$-term depends on the tidal solution. Having obtained an initial solution ζ_0 in which these secondary effects were neglected, we can evaluate $\hat{\zeta}_0$ from it to get an estimate of its magnitude:

$$\hat{\zeta}_0 = \alpha \sum \epsilon'_n \zeta_{0n}/(2n+1). \tag{18}$$

Figure 6 shows a map of $\hat{\zeta}_0$ derived from the initial solution for a sloping shelf model. The dashed lines are corange lines, and we note that some contour lines reach the value of 7.5 cm. On the right we have entered the amplitude of the effective equilibrium tide. It has a maximum value of 16.7 cm at the equator and decreases to zero towards the poles. Clearly $\hat{\zeta}_0$ is by no means negligibly small in comparison with $(1+k-h)\,\bar{\zeta}$ .What is even more serious is that the horizontal gradients of $\hat{\zeta}$, which alone enter the tidal equations, are comparable to those of $(1+k-h)\,\bar{\zeta}$, and in many places *exceed* them.

In spite of this alarming situation, the first iteration, with the gradients stemming from $\hat{\zeta}_0$ included, gives a solution ζ_1 not radically different from ζ_0. True, this first correction was substantial: $\langle|\zeta_1-\zeta_0|\rangle$ was 17 cm compared with $\langle|\zeta_0|\rangle \simeq 25$ cm, and $|\zeta_1-\zeta_0|_{\max}$ was 145 cm, but the global features of the tidal map were preserved. The reason for the relative ineffectiveness of the gradients of $\hat{\zeta}$ is that their *scale* is of the size of an amphidromic system, of which there are around a dozen, as against the *global* scale of $\bar{\zeta}$.

Further iterations showed slow convergence: the $|\zeta_\nu-\zeta_{\nu-1}|_{\max}$ in the subsequent three iterations were 105, 67, and 41 cm. These iterations were carried out on a 4° grid model in order to save computing time: 6 min per iteration for the 4° model as against 60 min for the 2° grid-model.

A substantial acceleration of the convergence was effected when we took note of the fact that the $\hat{\zeta}$-map rather closely resembled the ζ-map. Not only do the amphidromic systems coincide, but even more striking is the agreement in the cotidal lines.

PHILOSOPHICAL TRANSACTIONS OF THE ROYAL SOCIETY A MATHEMATICAL, PHYSICAL & ENGINEERING SCIENCES

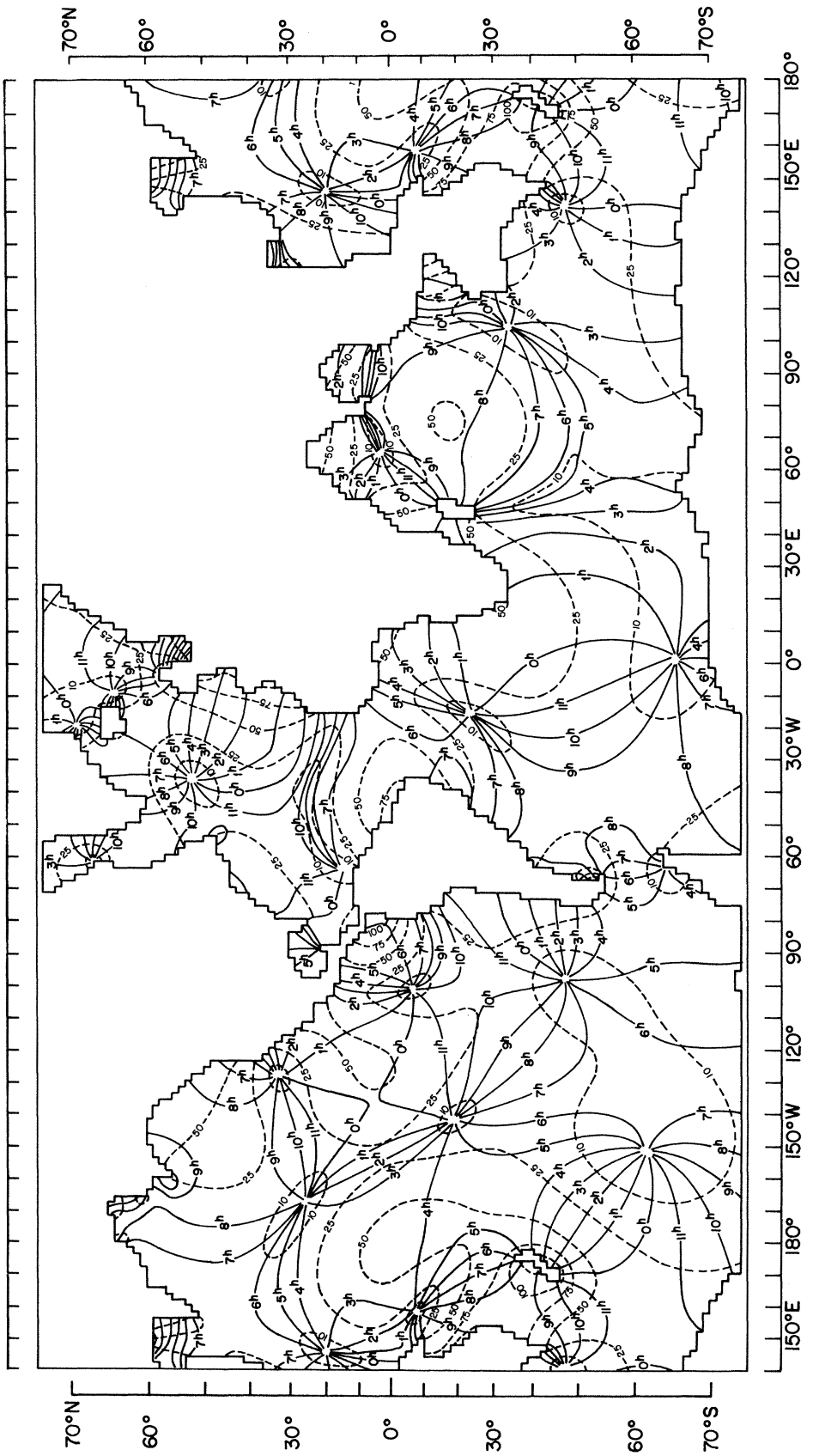

FIGURE 5. M_2 tide neglecting effects of self-attraction and of tidal loading. 2° grid, sloping shelf, $h' = 10$ m $S = 100$ km. ——, Cotidal lines (Greenwich hours); – – –, corange lines (units: cm).

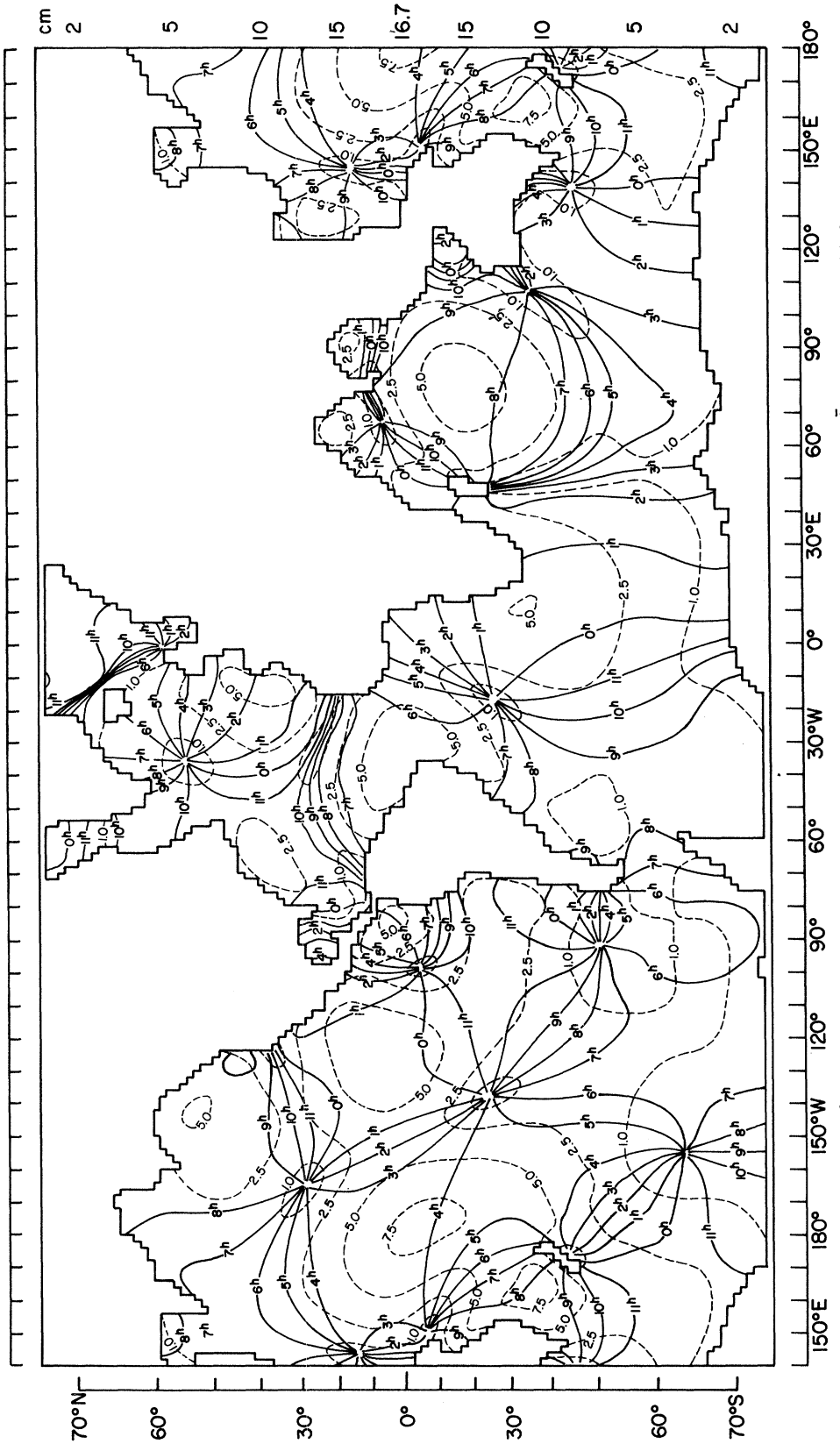

FIGURE 6. $\hat{\zeta} = -\Omega_1/g$. Ω_1 is the tidal potential due to self-attraction and to tidal loading, $\bar{\zeta}$ denotes the equilibrium tide. 2° grid, sloping shelf, $h' = 10$ m, $S = 100$ km. ----, Corange lines (units: cm).

This feature suggested representing $\hat{\zeta}$ as being proportional to ζ:

$$\hat{\zeta} = K\zeta + \Delta, \tag{19}$$

where Δ represents the residuals which are not correlated with ζ. A least-squares solution for the correlation coefficient K yields

$$K = \iint \hat{\zeta}\zeta^* \, dA \Big/ \iint \zeta\zeta^* \, dA, \tag{20}$$

where the integration is carried out over the surface of the ocean, and the star designates complex conjugate. As defined in (20), K could be complex, but because of the matching in phase between $\hat{\zeta}$ and ζ, pointed out earlier, K comes out to be almost real, and of the order of 0.085.

The procedure followed in the K-iterations is as follows. Having determined K_ν from the iteration of order ν, we write

$$\operatorname{grad} \hat{\zeta}_{\nu+1} = K_\nu \operatorname{grad} \zeta_{\nu+1} + \operatorname{grad} \Delta_\nu, \tag{21}$$

with

$$\Delta_\nu = \hat{\zeta}_\nu - K_\nu \zeta_\nu. \tag{22}$$

We include the term $K_\nu \operatorname{grad} \zeta_{\nu+1}$ with the main $\zeta_{\nu+1}$ terms in the tidal equations to be solved for, and treat only grad Δ_ν as the perturbation.

TABLE 1. CONVERGENCE OF THE ITERATIONS

K is the coefficient in the assumed relation $\hat{\zeta} = K\zeta + \Delta$, where $-g\hat{\zeta}$ denotes the tidal potential due to self-attraction and to tidal loading. $K = \iint \hat{\zeta}\zeta^* \, dA / \iint \zeta\zeta^* \, dA$. $\langle|\zeta|\rangle = 26.3$ cm. 4° grid. Sloping shelf, $h' = 10$ m, $S = 100$ km.

iteration ν	K	$\langle\lvert\zeta_\nu - \zeta_{\nu-1}\rvert\rangle$ cm	$\lvert\zeta_\nu - \zeta_{\nu-1}\rvert_{\max}$ cm	$K = 0$ $\langle\lvert\zeta_\nu - \zeta_{\nu-1}\rvert\rangle$ cm	$K = 0$ $\lvert\zeta_\nu - \zeta_{\nu-1}\rvert_{\max}$ cm
0	0.08507 + 0.00005i				
1	0.08652 + 0.00028i	15.7	116.4	17.2	144.7
2	0.08468 + 0.00025i	2.2	31.1	9.4	105.1
3	0.08482 + 0.00025i	0.43	8.1	5.5	67.4
4	0.08482 + 0.00025i	0.095	2.2	3.4	41.3

The results of the iteration by the K-method are shown in table 1. Note the substantial reality of K. At the fourth iteration with the K-method $\langle|\zeta_\nu - \zeta_{\nu-1}|\rangle$ was reduced to 1 mm and $|\zeta_\nu - \zeta_{\nu-1}|_{\max}$ to 2.2 cm.

Having thus found an efficient iterative procedure by experimenting with the 4° grid model, we applied the K-method to the 2° model, and the results are shown in table 2. The fourth iteration was carried out not because geophysical considerations require an accuracy of $\frac{1}{2}$ mm in the tidal elevation, but so as not to have to return to these computations again in the future.

Figure 7 gives the final solution for the Proudman model. The northeastern Pacific amphidrome moved off-shore, but not far enough. One notes the 25 cm corange line barely touching the coast at points far from La Jolla. In figure 8, which shows the final map for the sloping-shelf model, it is the 50 cm corange line that approaches the coast near La Jolla. Figure 9 shows the northeastern Pacific amphidrome produced by the sloping-shelf model. The location of the amphidromic centre agrees with that determined observationally. At La Jolla the observed phase is 4.8 h as against a theoretical value of 4.1 h. The observed and theoretical tidal amplitudes are 51 and 43 cm respectively. On the whole, the mean lead of the theoretical tide relative to the observed values has been reduced to near zero, with a mean scatter of about 1 h.

TABLE 2. CONVERGENCE OF THE ITERATIONS

is the coefficient in the assumed relation $\hat{\xi} = K\zeta + \Delta$, where $-g\hat{\xi}$ denotes the tidal potential due to self-attraction and to tidal loading. $K = \iint \hat{\xi}\zeta^* \, dA / \iint \zeta\zeta^* \, dA$. 2° grid.

	sloping shelf, $h' = 10$ m, $S = 100$ km			Proudman boundary condition, $h' = 25$ m		
ν	K	$\langle\lvert\zeta_\nu - \zeta_{\nu-1}\rvert\rangle$ cm	$\lvert\zeta_\nu - \zeta_{\nu-1}\rvert_{max}$ cm	K	$\langle\lvert\zeta_\nu - \zeta_{\nu-1}\rvert\rangle$ cm	$\lvert\zeta_\nu - \zeta_{\nu-1}\rvert_{max}$ cm
0	0.08821 − 0.00002i			0.09213 + 0.00066i		
1	0.08676 + 0.00027i	14.2	115.3	0.09284 + 0.00043i	14.6	93.2
2	0.08515 + 0.00022i	2.0	21.3	0.09190 + 0.00040i	1.3	11.4
3	0.08537 + 0.00023i	0.28	4.2	0.09194 + 0.00040i	0.17	1.3
4	0.08538 + 0.00023i	0.056	0.74			
		$\langle\lvert\zeta\rvert\rangle = 24.9$ cm			$\langle\lvert\zeta\rvert\rangle = 23.6$ cm	

6. COMPARISON WITH OBSERVATIONS

In carrying out the solution of the tidal equations, a computational grid of 2° was used. The sufficiency of the numerical convergence of the 2° solution was substantiated by comparing the results with those derived from a 4° solution. The Love numbers used are for the Gutenberg model, and are tabulated in appendix C.

The values of 25 and 10 m adopted for the parameter h' in the Proudman and sloping-shelf models respectively are not critical. The dissipation is insensitive to moderate changes in h', for the reason that when h' is increased, the amplitude of the tide decreases, resulting in a relatively smaller change in the dissipation.

Figure 10 gives a comparison between observed and theoretical tidal values for the northeastern Pacific coast. The upper curve gives a comparison of the phases, which are seen to be in reasonable agreement with observed values. The tidal amplitudes, shown in the lower part of figure 10, are in good agreement south of latitude 50° N. To the north, in the region of the Alexander archipelago, the observed tidal amplitudes reach values of 180 cm, whereas the theoretical values reach only 80 cm. Possibly we have here a manifestation of the *fiord-effect*: the local amplification of the tide in confined bays.

Figure 11 gives a comparison of the observed tides with the calculated values along the western Atlantic coast. The phases, shown in the upper figure, are in good agreement with observations. Note the typical jump in the phases on passing through the Caribbean amphidrome. The observed amplitudes are higher than the theoretical ones, especially where the former reach values of around 100 cm.

Figure 12 gives a comparison of observed with theoretical tidal values along the western Pacific coast. The theoretical phases are satisfactory except in the Coral Sea, where the amplitudes are also not reproduced satisfactorily.

An interesting feature of the tides around New Zealand is that the phases at stations lying across the narrow width of the islands differ by about 6 h, as if New Zealand were the centre of an amphidrome, with the amplitudes at the centre being a maximum rather than a minimum (zero). The theoretical tides bring out this feature; indeed, it already appeared in the solution of I (figure 10). Figure 14 gives a comparison between observed and theoretical tides for the coastal stations shown in figure 13. The theoretical amplitudes are satisfactory, while the theoretical phases are in

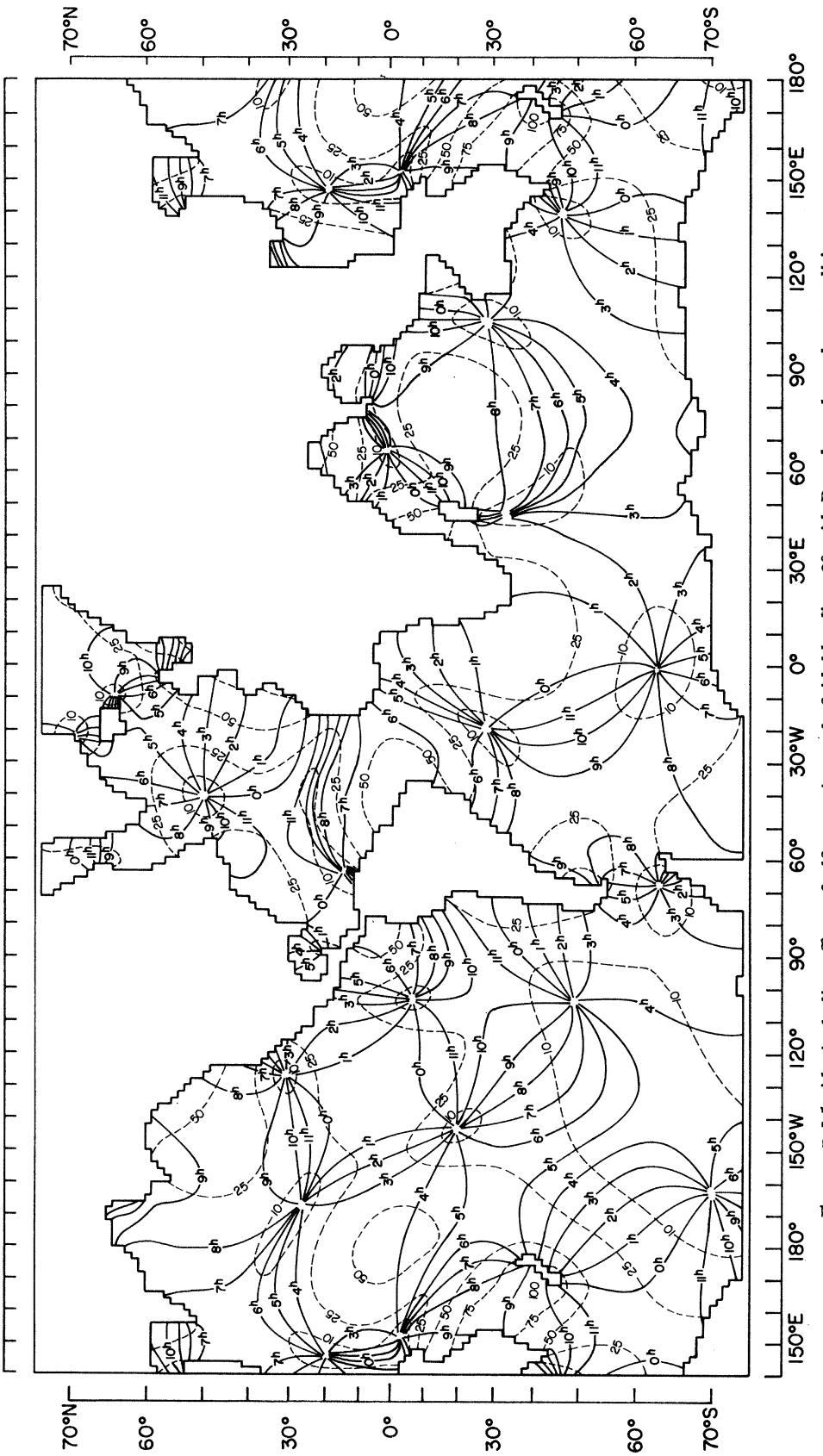

FIGURE 7. M_2 tide, including effects of self-attraction and of tidal loading. 2° grid, Proudman boundary condition, $h' = 25$ m. ——, Cotidal lines (Greenwich hours); – – –, corange lines (units: cm).

PHILOSOPHICAL TRANSACTIONS OF THE ROYAL SOCIETY A MATHEMATICAL, PHYSICAL & ENGINEERING SCIENCES

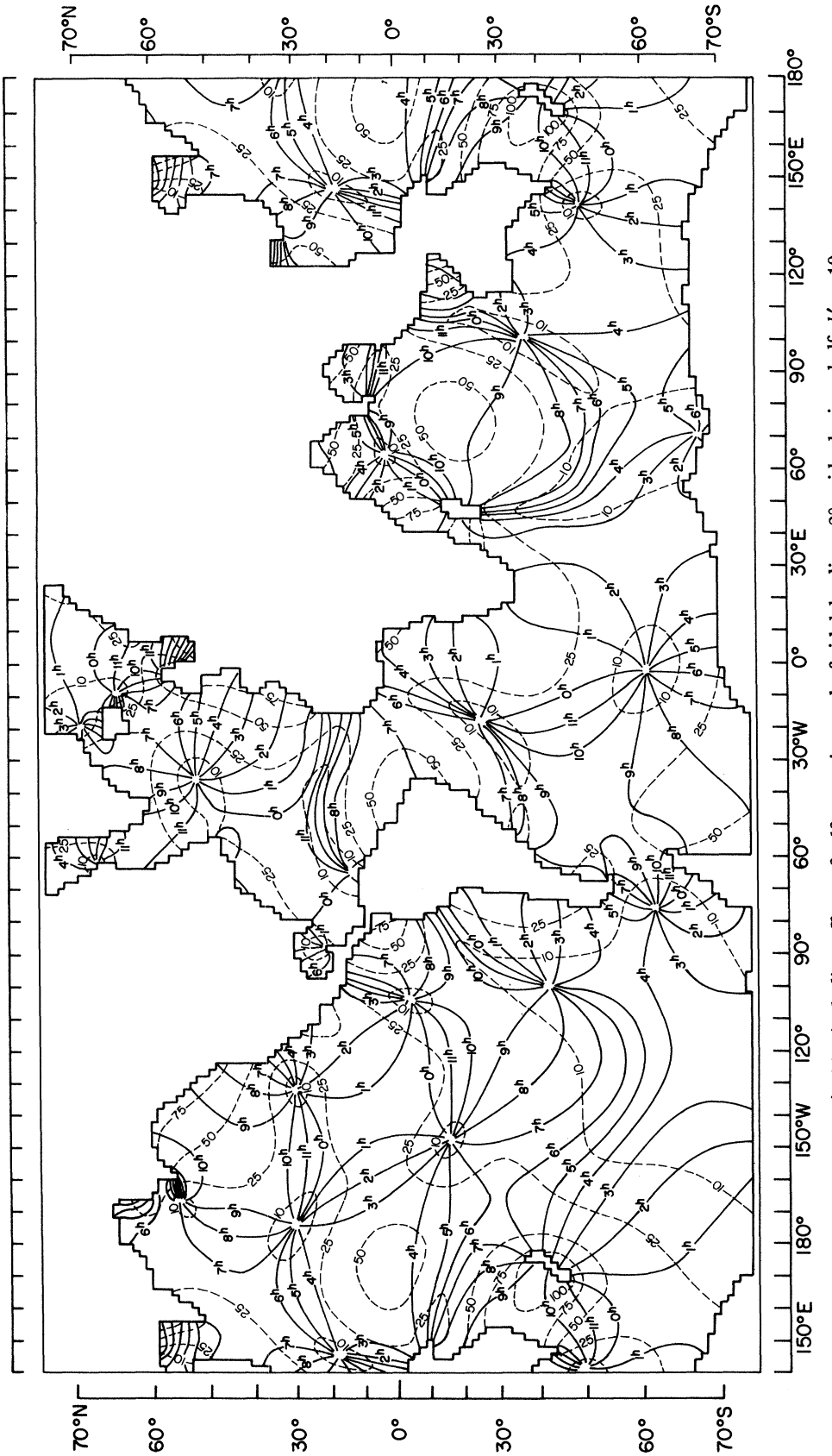

FIGURE 8. M_2 tide, including effects of self-attraction and of tidal loading. 2° grid, sloping shelf, $h' = 10$ m, $S = 100$ km. ——, Cotidal lines (Greenwich hours); – – –, corange lines (units: cm).

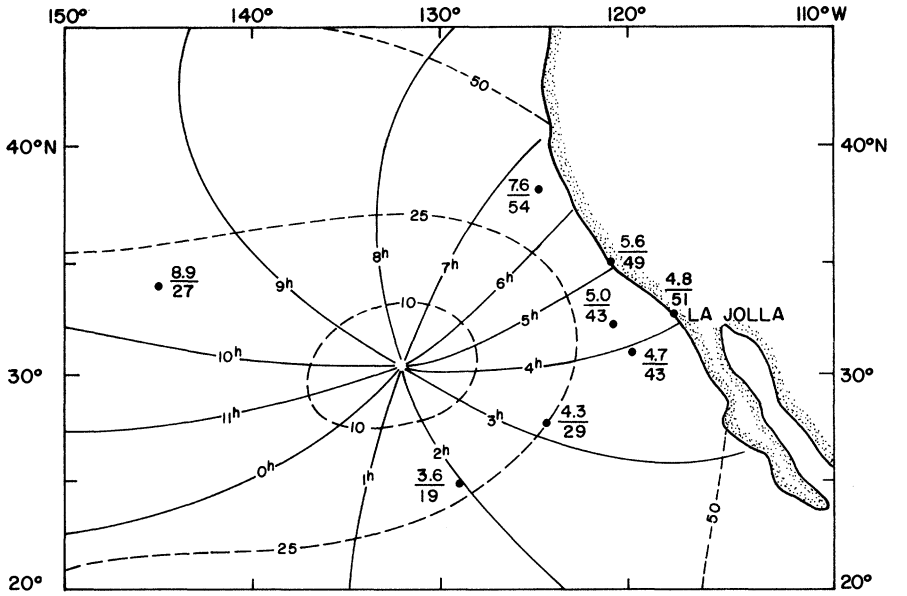

FIGURE 9. M_2 amphidrome in the northeast Pacific. Observed values (time/amplitude) taken from Irish *et al.* (1971).

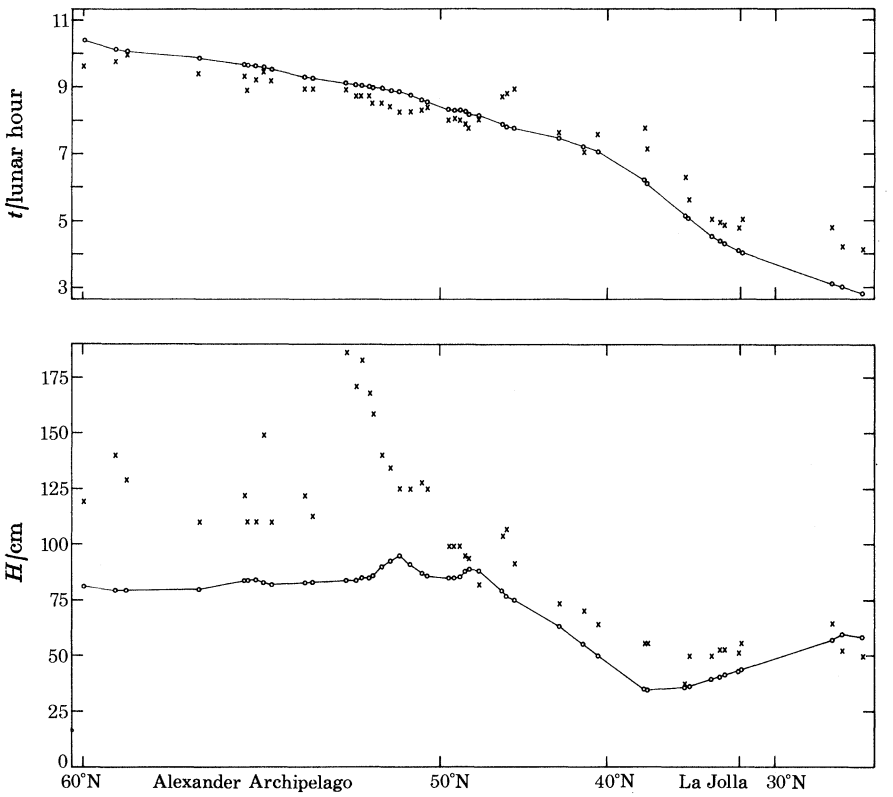

FIGURE 10. Comparison of observed with theoretical tides along the northeastern Pacific coast. ×, Observed; o, theoretical.

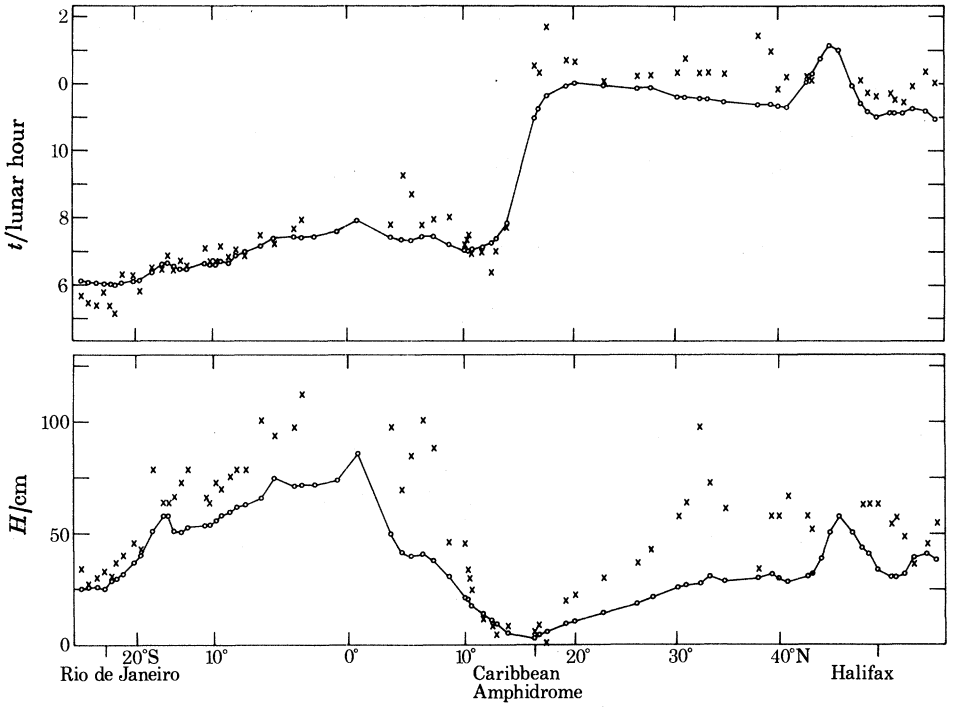

FIGURE 11. Comparison of observed with theoretical tides along the western Atlantic. ×, Observed; ○, theoretical.

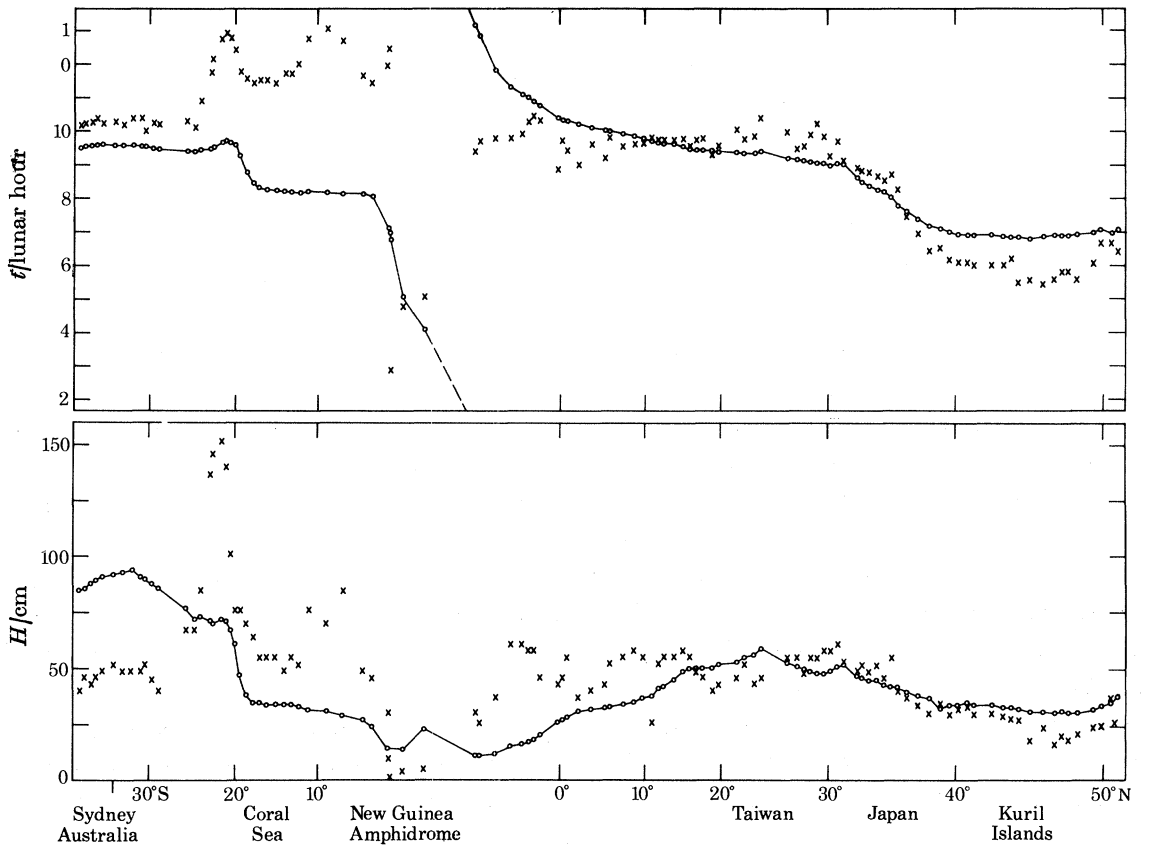

FIGURE 12. Comparison of observed with theoretical tides along the western Pacific coast. ×, Observed; ○, theoretical.

advance of the observed values by about 1 h, on average. Note that in the model, the two islands were joined.

In the island stations shown in table 3, we give our solution both for a rough boundary (figure 8) and for a smooth boundary (figure 18). In the south Atlantic and in the Indian Ocean, the agreement of both amplitudes and phases with observations is good. Elsewhere, the agreement is

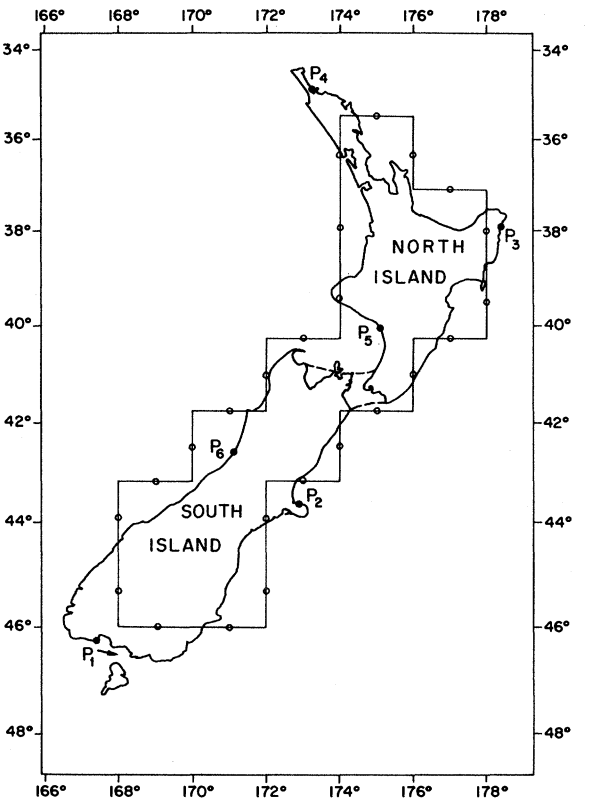

FIGURE 13. The New Zealand coast $P_1 \ldots P_6$, and the neighbouring grid-points.

satisfactory, except for the south Pacific Ocean, where, however, the topography of the ocean bottom is still largely uncertain.

The islands chosen are identical with those listed in table 3 of I, except for an additional two stations near Honolulu, taken from Larsen (1977). For comparison, the theoretical amplitudes in I should be multiplied by a factor 0.69 stemming from the yielding of the Earth to the direct tidal potential. Note several changes in the observed values based on more recent measurements.

The changes introduced by including the secondary effects due to tidal loading and to tidal self-attraction are illustrated in table 4 and in figure 15. The change in the tidal amplitudes is small, but there is an improvement in the phases, in the sense that the mean of the deviation $(t_{\mathrm{obs}} - t_{\mathrm{th}})$ is reduced to near zero.

As for the S_2 tide shown in figure 16, there is no evidence for resonance at the semidiurnal period (Jeffreys 1975), the average of the ratio of the theoretical amplitudes of S_2 to M_2 being close to the ratio of the respective amplitudes of the equilibrium tides.

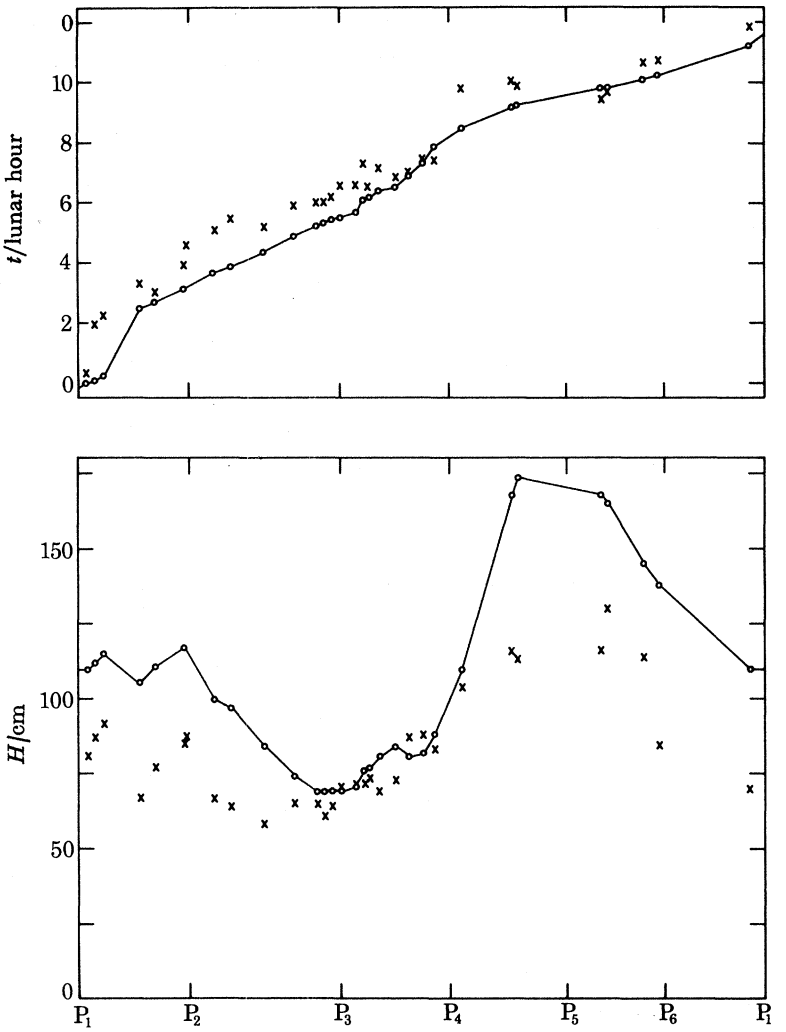

FIGURE 14. Comparison of observed wth theoretical tides on the New Zealand coast. ×, Observed; ○, theoretical.

7. TIDAL DISSIPATION AND THE DECELERATING COUPLE EXERTED BY THE TIDE-PRODUCING BODY ON THE EARTH

The force per unit mass exerted by the tidal potential $\bar{\Omega}$ in the direction of increasing longitude λ is $-(1/r\sin\theta)\,\partial\bar{\Omega}/\partial\lambda$. The moment of this force per unit volume is therefore $-\rho\partial\bar{\Omega}/\partial\lambda$. Integrating $-\rho\partial\bar{\Omega}/\partial\lambda$ over the (variable) volume of the ocean we obtain the total decelerating moment N exerted by the tide-producing body on the Earth:

$$N = -\rho\iint\langle\zeta\,\partial\bar{\Omega}/\partial\lambda\rangle\,\mathrm{d}A, \tag{23}$$

where $\mathrm{d}A$ is an element of the surface of the ocean. For the semidiurnal tide given in equations (2) and (3) we have from (23)

$$N = 24.25\,g\rho a^2\int\mathrm{d}\theta\int\mathrm{d}\lambda|\zeta|\sin^3\theta\sin(2\lambda-\gamma), \tag{24}$$

PHILOSOPHICAL TRANSACTIONS OF THE ROYAL SOCIETY A MATHEMATICAL, PHYSICAL & ENGINEERING SCIENCES

TABLE 3. COMPARISON OF TIDAL OBSERVATIONS ON ISLANDS, WITH THEORETICAL VALUES

(H is the amplitude of the M_2 tide, and t denotes the phase lag, r – rough coastline, s – smooth coastline)

station and area	ref.†	latitude	longitude	H_{obs} cm	$H_{th(r)}$ cm	$H_{th(s)}$ cm	t_{obs} h	$t_{th(r)}$ h	$t_{th(s)}$ h
North Atlantic Ocean									
Flores I., Azores	2204	39° 23′ N	31° 11′ W	39	27	34	2.0	1.9	1.8
Santa Maria I., Azores	2203	36° 57′ N	25° 09′ W	51	40	48	2.0	2.1	2.1
Funchal, Madeira	377	32° 38′ N	16° 54′ W	72	60	71	1.5	1.9	1.8
Tenerife, Canary I.	2317	28° 29′ N	16° 14′ W	69	61	70	1.0	1.4	1.3
Santo Antao, Cape Verde I.	2204	17° 01′ N	25° 04′ W	30	18	21	8.7	9.4	9.2
Eleuthera I., Bahama I.	2212	24° 56′ N	76° 09′ W	32	19	20	0.7	11.8	11.7
St George's I., Bermuda	2170	32° 24′ N	64° 42′ W	37	21	24	0.0	11.4	11.5
South Atlantic Ocean									
Ascension I.	C	7° 55 S	14° 25′ W	33	23	27	5.9	5.9	6.0
Fernando de Noronha	1040	3° 50′ S	32° 24′ W	79	59	70	6.9	7.0	7.0
St Helena I.	C	15° 55′ S	5° 42′ W	32	23	27	2.7	2.4	2.4
Isla Trinidade	C	20° 30′ S	29° 20′ W	33	28	33	7.0	6.5	6.8
Tristan da Cunha	C	37° 02′ S	12° 18′ W	23	23	25	0.4	0.3	0.3
Stanley Harbour, Falkland I.	2321	51° 42′ S	57° 51′ W	45	24	31	9.1	9.1	9.1
Elsehul, South Georgia	1101	54° 02′ S	38° 00′ W	27	20	22	9.0	9.2	9.1
Scotia Bay, South Orkney I.	2321	60° 44′ S	44° 39′ W	46	28	30	8.7	8.9	8.8
Indian Ocean									
Port Victoria, Seychelles I.	2137	4° 37′ S	55° 27′ E	40	31	35	0.4	0.8	0.4
Port Louis, Mauritius	24	20° 09′ S	57° 29′ E	13	42	43	8.9	9.2	8.9
Addu Atoll	1099	0° 34′ S	73° 13′ E	29	33	36	8.4	9.2	8.5
Port Refuge, Cocos I.	2208	12° 05′ S	96° 53′ E	27	28	31	10.4	10.1	9.5
St Paul I.	2196	38° 43′ S	77° 35′ E	38	29	36	7.7	8.5	8.0
Port-aux-Francais, Kerguelen	2348	49° 21′ S	70° 13′ E	51	12	16	6.5	7.2	6.8
North Pacific Ocean									
Pagan I., Marianas I.	3048	18° 08′ N	145° 46′ E	17	1	2	9.8	3.5	4.1
Kusaie I., Caroline I.	3049	5° 20′ N	163° 01′ E	42	54	49	4.3	3.5	3.3
Port Rhin, Marshall I.	3048	6° 14′ N	171° 48′ E	57	59	55	4.4	3.6	3.6
Midway I.	2210	28° 12′ N	177° 22′ W	11	9	6	3.0	3.7	4.2
Johnston I.	2167	16° 45′ N	169° 30′ W	27	28	23	3.5	2.7	3.0
Honolulu, Hawaiian I.	L	21° 18′ N	157° 52′ W	16	19	16	2.1	0.6	0.1
Kahului, Hawaiian I.	L	20° 54′ N	156° 28′ W	18	20	18	0.4	0.5	0.1
Hilo, Hawaiian I.	L	19° 44′ N	155° 04′ W	21	23	20	1.0	0.6	0.3
South Pacific Ocean									
Lord Howe I., Tasman Sea	940	31° 32′ S	159° 04′ E	59	96	33	10.1	9.4	9.0
Paagoumene Bay, New Caledonia	2147	20° 29′ S	164° 11′ E	45	45	47	9.0	8.2	8.3
Vila Harbour, New Hebrides	1095	17° 45′ S	168° 19′ E	34	34	34	6.9	7.2	7.3
Kingston, Norfolk I.	2232	29° 04′ S	167° 56′ E	57	78	79	8.8	8.7	8.3
Nukualofa, Tonga I.	1092	21° 08′ S	175° 13′ W	52	36	45	6.4	6.0	5.9
Funafuti, Ellice I.	2172	8° 32′ S	179° 12′ E	57	49	50	5.1	4.3	4.5
Aitutaki, Cook I.	2233	18° 51′ S	159° 47′ W	17	24	32	7.0	5.6	5.6
Hanga Piko, Easter I.	948	27° 09′ S	109° 27′ W	21	18	12	0.5	9.5	10.0
Caleta Aeolian, Galapagos I.	2168	0° 26′ S	90° 17′ W	72	40	49	8.2	7.3	7.3
Gambier I., Polynesian Arch.	2348	23° 07′ S	134° 58′ W	27	18	12	11.6	9.2	9.0
Ahe, Polynesian Arch.	2347	14° 32′ S	146° 21′ W	12	4	4	2.9	0.1	4.1
Nukuhiva, Polynesian Arch.	2260	8° 55′ S	140° 06′ W	47	25	21	1.2	0.3	0.6

† number – I.H.B., C – Cartwright 1971, L – Larsen 1977.

PHILOSOPHICAL TRANSACTIONS OF THE ROYAL SOCIETY A MATHEMATICAL, PHYSICAL & ENGINEERING SCIENCES

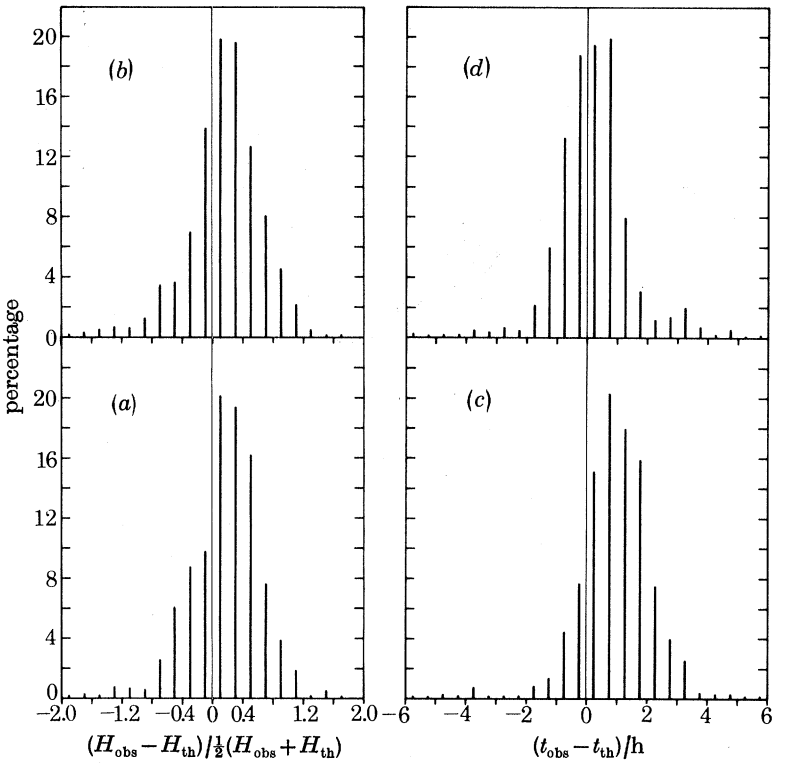

FIGURE 15. Statistics of deviation of theoretical from observed M_2 tidal amplitudes and phases. Sloping shelf, $h' = 10$ m, $S = 100$ km, (a) and (c): neglecting secondary effects. (b) and (d): including secondary effects.

TABLE 4. DIFFERENCES BETWEEN THEORETICAL AND OBSERVED TIDAL VALUES

	number of stations	neglecting secondary effects				including secondary effects			
		$\langle\Delta H\rangle$	$\langle\lvert\Delta H\rvert\rangle$	$\langle\Delta t\rangle$	$\langle\lvert\Delta t\rvert\rangle$	$\langle\Delta H\rangle$	$\langle\lvert\Delta H\rvert\rangle$	$\langle\Delta t\rangle$	$\langle\lvert\Delta t\rvert\rangle$
coastal stations									
Eastern Pacific coast	114	0.33	0.41	1.4	1.4	0.29	0.32	0.2	0.6
Western Atlantic coast	170	0.28	0.39	0.9	1.1	0.46	0.52	0.2	0.8
Greenland	9	0.77	0.77	−0.2	0.2	0.88	0.88	−1.3	1.3
Eastern Atlantic and Western Indian Ocean	153	0.20	0.27	0.5	0.5	0.22	0.26	−0.4	0.6
Madagascar	12	0.40	0.55	0.6	1.1	0.16	0.36	−0.5	0.8
Indian Ocean coast (Arabian Sea – Tasmania)	156	0.12	0.46	0.9	1.6	0.05	0.48	−0.2	1.1
Western Pacific (Tasmania – Bering)	348	0.10	0.37	0.8	1.2	0.06	0.35	0.4	1.1
New Zealand	41	−0.32	0.33	1.9	1.9	−0.23	0.26	0.9	0.9
Island stations									
North Atlantic	43	0.31	0.34	0.9	0.9	0.43	0.43	−0.1	0.5
Mid South Atlantic	11	0.35	0.36	0.6	0.6	0.28	0.28	0.0	0.2
South-West Atlantic	12	0.83	0.83	1.6	1.6	0.71	0.71	0.3	0.6
North Pacific	94	0.13	0.46	0.7	1.5	−0.04	0.45	0.2	1.2
South Pacific	97	−0.06	0.43	1.0	1.7	−0.10	0.46	0.6	1.1
Indian Ocean	19	0.25	0.52	1.2	1.2	0.19	0.52	0.0	0.7
average	1279	0.16	0.39	0.9	1.0	0.15	0.40	0.2	0.9

$\Delta H = (H_{obs}-H_{th})/\frac{1}{2}(H_{obs}+H_{th})$, $\Delta t = t_{obs}-t_{th}$ (in hours)

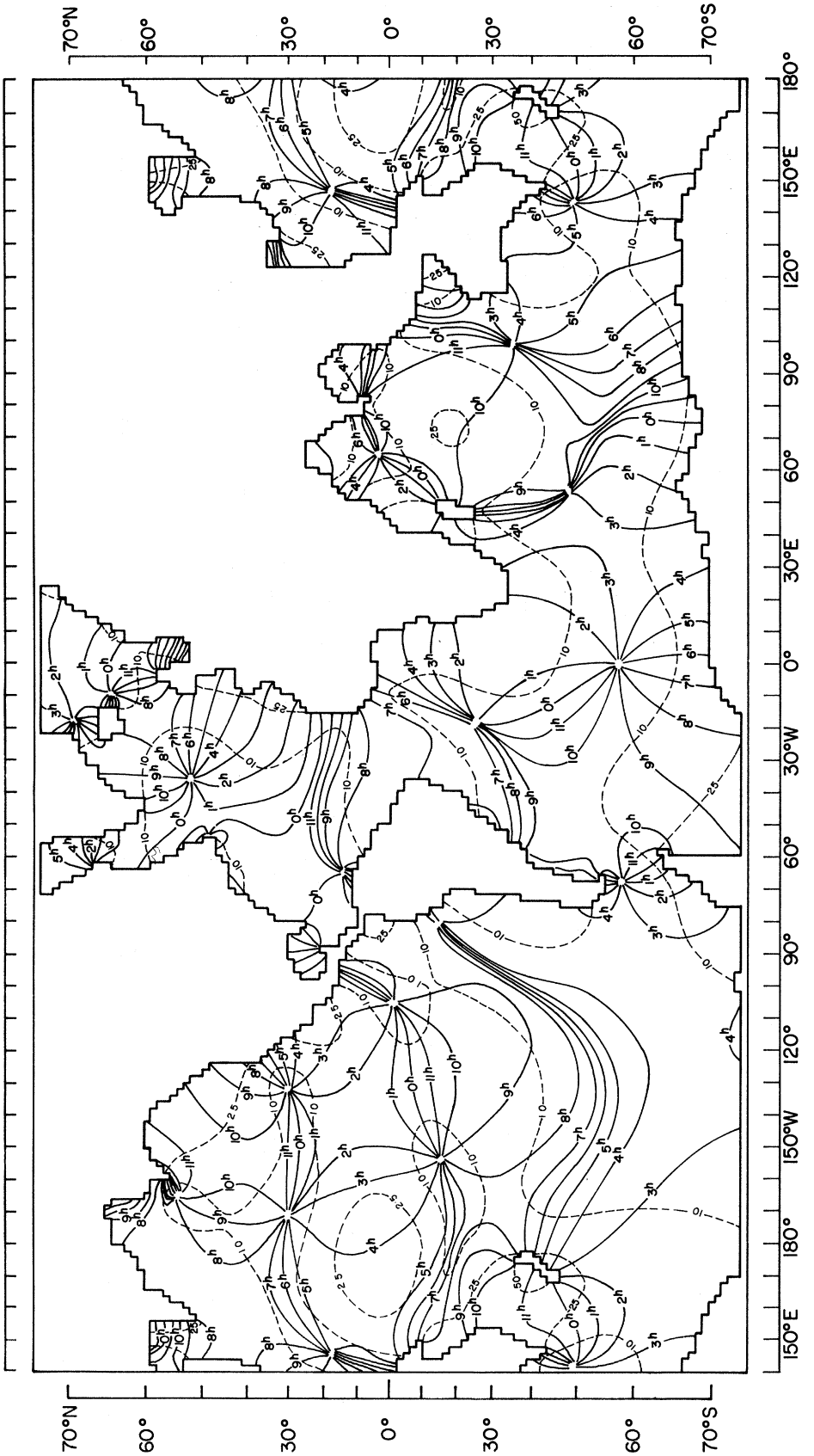

FIGURE 16. S_2 tide, including effects of self-attraction and of tidal loading. 2° grid, sloping shelf, $h' = 10$ m, $S = 100$ km. ——, Cotidal lines (Greenwich hours); – – –, corange lines (units: cm).

PHILOSOPHICAL TRANSACTIONS OF THE ROYAL SOCIETY A MATHEMATICAL, PHYSICAL & ENGINEERING SCIENCES

where γ is the phase of the tide ζ. The sine term in (24) stems from the relation

$$\langle \cos(\sigma t+\gamma)\sin(\sigma t+2\lambda)\rangle = \tfrac{1}{2}\sin(2\lambda-\gamma). \tag{25}$$

Clearly, the retarding couple is due to the difference between the phase of the tide γ and the phase of the tidal potential 2λ.

In both the Proudman model and the sloping-shelf model, the tidal dissipation occurs on the coasts. We have for the dissipation D in the Proudman model

$$\begin{aligned} \mathrm{d}D_{\mathrm{P}} &= \langle \delta p u_{\mathrm{n}}\rangle h\,\mathrm{d}l = \langle \rho g\zeta u_{\mathrm{n}}\rangle h\,\mathrm{d}l \\ &= \rho g\sqrt{(h'g)}\,\langle\zeta^2\rangle\,\mathrm{d}l, \end{aligned} \tag{26}$$

$$D_{\mathrm{P}} = \rho g\int \mathrm{d}l\sqrt{(h'g)}\,\langle\zeta^2\rangle, \tag{27}$$

where $\mathrm{d}l$ denotes integration along the coast.

Similarly, we have, by (17), for the dissipation in the sloping-shelf model

$$D_{\mathrm{slsh}} = \rho g\int \mathrm{d}l\sqrt{(hg)}\,\mathrm{Re}\left(\frac{1-R}{1+R}\right)\langle\zeta^2\rangle. \tag{28}$$

Let the couples exerted by the Moon and Sun on the Earth be denoted by N and N' respectively, and let n and n' denote their respective angular orbital velocities around the Earth; then, with C denoting the moment of inertia of the Earth about its axis of rotation, we have (Jeffreys 1976, p. 318)

$$C\,\mathrm{d}\omega/\mathrm{d}t = -N-N', \tag{29}$$

$$-\mathrm{d}E/\mathrm{d}t = (N+N')\,\omega - Nn - N'n'. \tag{30}$$

Here E denotes the total mechanical energy of the system Earth–Moon–Sun. With

$$n = 2.66\times10^{-6}\,\mathrm{s}^{-1},\quad n' = 1.99\times10^{-7}\,\mathrm{s}^{-1},\quad \omega = 7.29\times10^{-5}\,\mathrm{s}^{-1}, \tag{31}$$

and the values

$$N = 3.48\times10^{23}\,\mathrm{dyn\,cm},\quad N' = 0.700\times10^{23}\,\mathrm{dyn\,cm}, \tag{32}$$

given in table 5, equation (30) reads

$$-\mathrm{d}E/\mathrm{d}t = (3.048-0.0926-0.0014)\times10^{19}\,\mathrm{erg/s}, \tag{33}$$

$$\mathrm{d}E/\mathrm{d}t = -2.95\times10^{19}\,\mathrm{erg/s}. \tag{34}$$

This value is within 4 % of the values of 3.08×10^{19} erg/s given in table 5, and compares well with Jeffreys's estimate of 2.9×10^{19} erg/s (Jeffreys 1976, p. 338). If we consider the different

TABLE 5. TIDAL DISSIPATION D AND TIDAL RETARDING MOMENT N

	dissipation, D / 10^{19} erg/s	retarding moment, N / 10^{23} dyn cm	D/N / 10^{-5} s^{-1}
M_2 2° Proudman, $h' = 25$ m	2.60	3.82	6.8
M_2 2° Proudman, K, $h' = 25$ m	2.44	3.42	7.1
M_2 2° slope, $h' = 10$ m, $S = 100$ km	2.79	3.95	7.1
M_2 2° slope, K, $h' = 10$ m, $S = 100$ km	2.55	3.48	7.3
S_2 2° slope, K, $h' = 10$ m, $S = 100$ km	0.526	0.700	7.51
M_2+S_2 2° slope, K, $h' = 10$ m, $S = 100$ km	3.08	4.18	7.37

$\omega = 7.29\times10^{-5}$ s^{-1}

nature of the surface-integral (24) for the couples and the line integrals (27) and (28) for the dissipation, it is striking that the ratio D/N given in table 5 comes out so close to the value of ω. The reason for this becomes clear by inspection of equation (33), showing that 97 % of the dissipation goes into slowing down the rotation of the Earth.

From equation (29), with

$$C = 8.022 \times 10^{44}\,\mathrm{g\,cm^2}, \quad N + N' = 4.18 \times 10^{23}\,\mathrm{dyn\,cm}, \tag{35}$$

it would follow that, as a result of the retarding action exerted by the M_2 and S_2 tides, there is currently a deceleration of the Earth's rotation of

$$\dot{\omega}/\omega = -2.26 \times 10^{-10}\,\mathrm{a^{-1}}, \quad \dot{\omega} = -1080''\,\mathrm{cy^{-2}}. \tag{36}$$

8. Summary

A model of the ocean's bottom topography was constructed on the basis of the more than one million soundings published by Dishon & Heezen (1968), and supplemented by interpolations in lacunary areas. Tidal dissipation was assumed to be of the albedo type either as in the Proudman model shown in figure 2, or as in the sloping-shelf model shown in figure 3. In both models there exists a proportionality between the component of tidal velocity normal to coast u_n and the tidal elevation ζ on the coast, as expressed in equations (16) and (17). These were used as boundary conditions on the coastline. The inclusion of the secondary effects due to tidal self-attraction and to tidal loading effected a correction of the order of 10 %, tending to improve the agreement of the theoretical tidal values with observations. The change due to the secondary effects is shown by comparing figure 4 with figure 7, and figure 5 with figure 8, for the Proudman and the sloping-shelf dissipation models respectively. The sloping-shelf model proved to be the more satisfactory one. A comparison between theoretical and observed tides is given in figures 9, 10, 11, 12, 14 and in table 3. The theoretical tidal phases scatter around the observed phases by about 1 h, and this after an improvement of about 1 h effected by the inclusion of the secondary effects. There are, however, regions of poor agreement with theory, especially in fiorded zones and in shallow seas. In addition, the situation with the gravity tide is not satisfactory. Possibly these shortcomings are due, in part, to inadequate representation of the topography of the bottom. The secondary effects on the M_2 tide were treated by Gordeev *et al.* (1977) and by R. H. Estes (unpublished).

The solution for the S_2 tide shown in figure 16 resembles the solution for the M_2 tide shown in figure 8, the average ratio of the theoretical amplitudes being close to the ratio of the amplitudes of the respective equilibrium tides.

On the question of the adequacy of the finite difference scheme of solution, especially with regard to the sharp corners introduced on the coast, we have the evidence from the solution for the 'smooth' coast shown in figures 17 and 18. Comparing the solution for the rough coastline shown in figure 8 with the solution for the smooth coastline shown in figure 18, we find that the tidal amplitudes are close, whereas the phases for the smooth coastline are in advance of those for the rough coastline by about $\frac{1}{4}$ h.

The total dissipation of 3.08×10^{19} erg/s comprises the contributions from the M_2 and S_2 tides. Assuming that the remaining semidiurnal tides of smaller amplitude all have the same appearance as the M_2 and S_2 tides shown in figures 8 and 16, we can estimate their contribution to the dissipation on the basis of an assumed amplitude square law. This comes out to be no more than

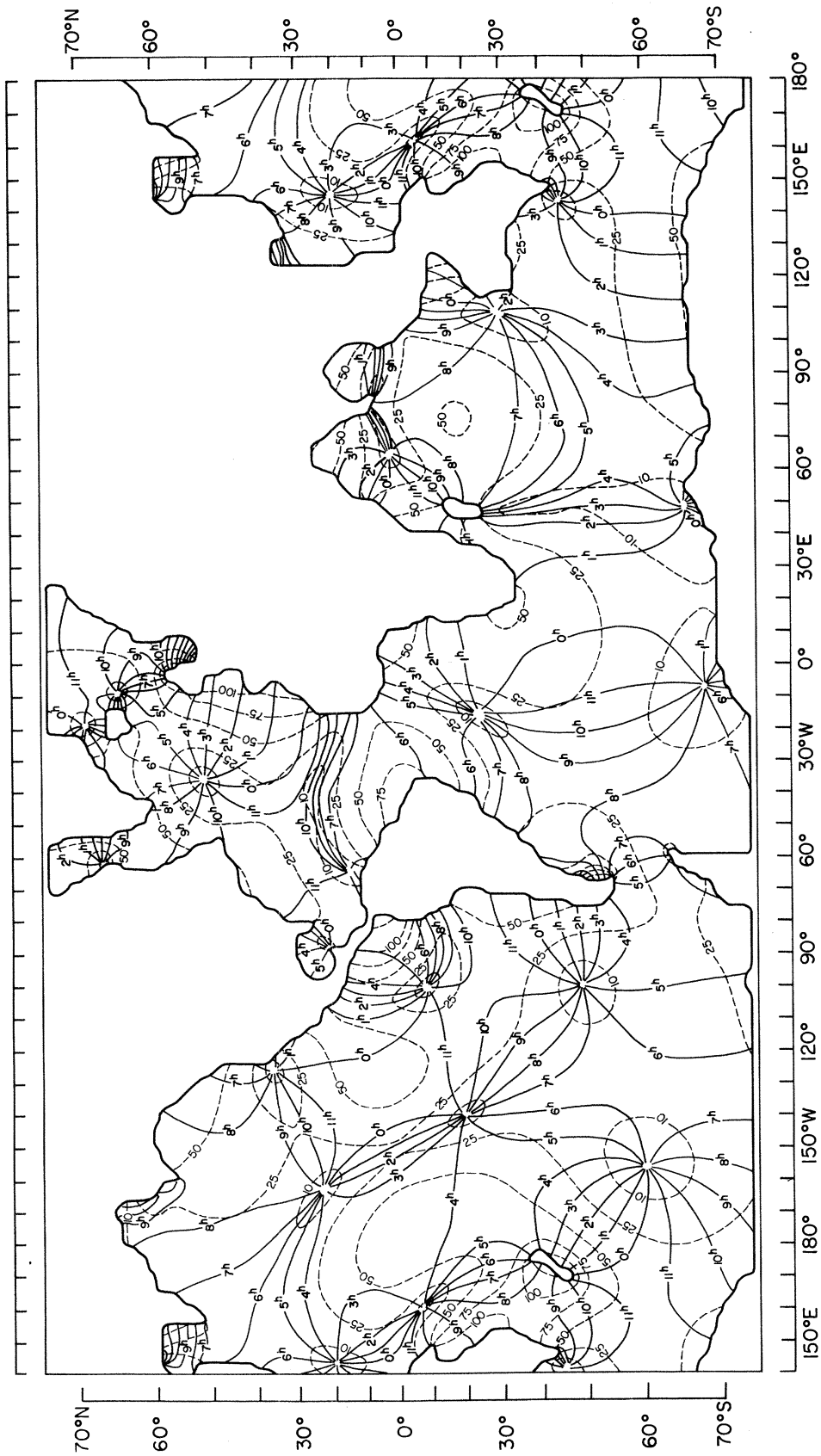

FIGURE 17. M_2 tide for smooth coastline neglecting effects of self-attraction and of tidal loading. 2° grid, sloping shelf, $h' = 10$ m, $S = 100$ km. ——, Cotidal lines (Greenwich hours); – – –, corange lines (units: cm).

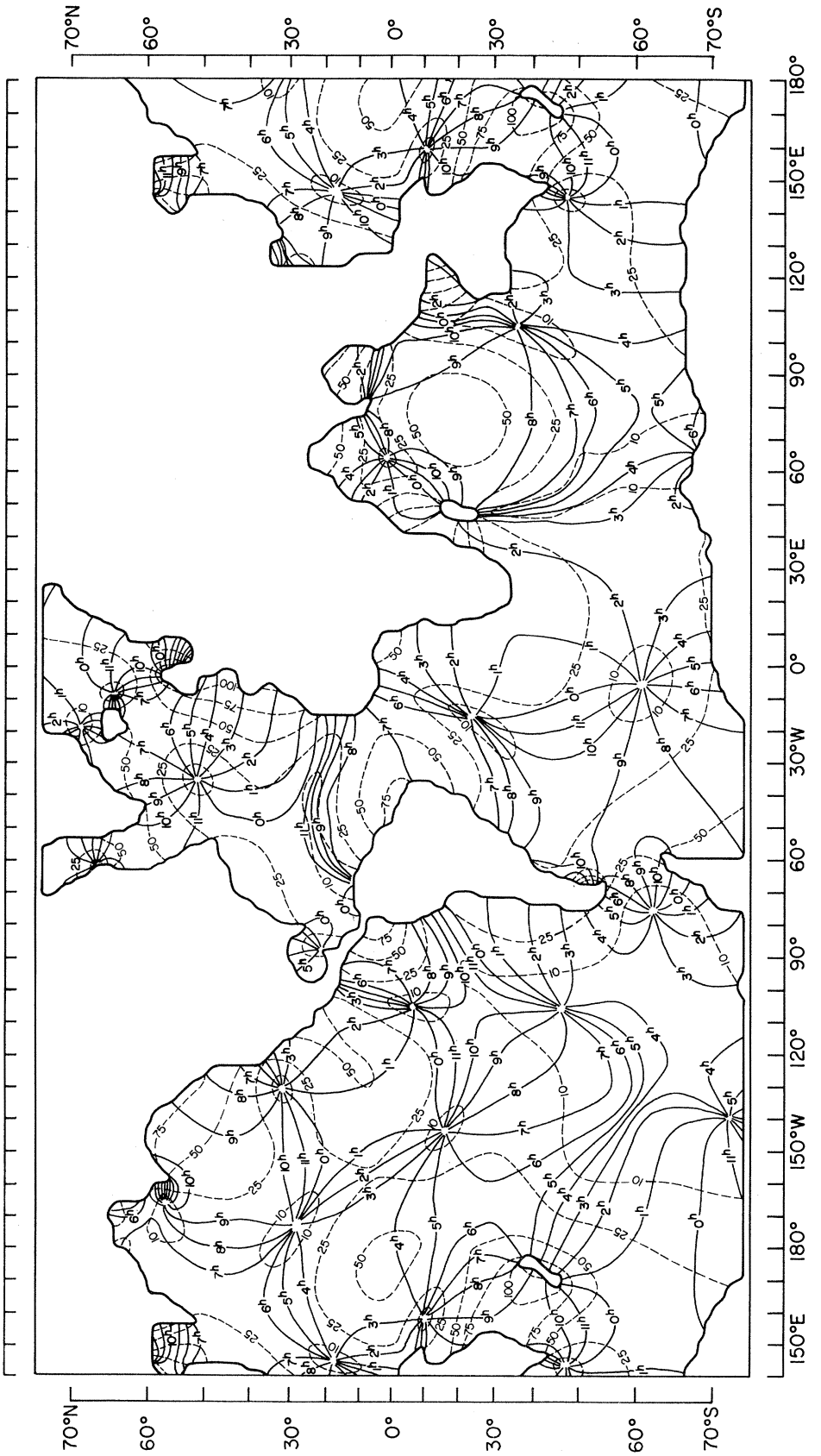

FIGURE 18. M_2 tide for smooth coastline including effects of self-attraction and of tidal loading. 2° grid, sloping shelf, $h' = 10$ m, $S = 100$ km. ——, Cotidal lines (Greenwich hours); – – –, corange lines (units: cm).

4%. The contribution from the diurnal tides must await their solution, but is probably not substantial.

Our theoretical value of about 6×10^{19} erg/s given in I has to be reduced by the factor $(0.69)^2 = 0.48$ to take account of the elastic yielding of the Earth to the tidal potential.† This reduction was pointed out by Jeffreys (1970). The theoretical rate of retardation of the Earth's rotation of $1080''/\text{cy}^2$ is in line with the currently accepted values (Jeffreys 1976, pp. 336–337).

This research was supported in part by the Office of Naval Research through contract N00014-76-C-0186.

Appendix A. Reflexion of the tide from a sloping shelf

We consider a long wave incident normally on a sloping shelf, as shown in figure 3. The wave propagates in the positive x-direction and the dissipation is represented by the tidal energy carried away in the channel of depth h'. Between $x = 0$ and $x = S$ the depth of the water H changes linearly from an initial value of h to a final value h':

$$H(x) = h - \gamma x, \quad 0 \leqslant x \leqslant S, \tag{A 1}$$

$$\gamma = (h - h')/S. \tag{A 2}$$

Because of the sloping bottom, the incident wave is partly reflected, and the tidal height ζ is represented, for a unit amplitude of the incident wave, by

$$\zeta = \mathrm{e}^{-\mathrm{i}kx} + R\mathrm{e}^{\mathrm{i}kx}, \quad x \leqslant 0, \tag{A 3}$$

where R denotes the complex reflexion coefficient, and a time factor $\mathrm{e}^{\mathrm{i}\sigma t}$ has been assumed. Equation (A 3) is a solution of the governing wave equation (Lamb 1932, p. 275)

$$-\sigma^2\zeta = g\frac{\partial}{\partial x}\left(H\frac{\partial\zeta}{\partial x}\right), \tag{A 4}$$

for constant depth, with

$$k = \sigma/(gh)^{\frac{1}{2}}. \tag{A 5}$$

In the region of the sloping bottom, equation (A 4) becomes

$$H\frac{\mathrm{d}^2\zeta}{\mathrm{d}H^2} + \frac{\mathrm{d}\zeta}{\mathrm{d}H} + \beta^2\zeta = 0, \quad 0 \leqslant x \leqslant S, \tag{A 6}$$

$$\beta^2 = \sigma^2/(\gamma^2 g), \tag{A 7}$$

whose solution is

$$\zeta = AJ_0(y) + BY_0(y), \tag{A 8}$$

with

$$y(x) = 2\beta\sqrt{(H(x))}. \tag{A 9}$$

In the shallow portion of the channel the solution is

$$\zeta = D\mathrm{e}^{-\mathrm{i}k'x}, \quad x \geqslant S, \tag{A 10}$$

where

$$k' = \sigma/(gh')^{\frac{1}{2}}. \tag{A 11}$$

† Lambeck (1977, table 5) applies only the factor 0.69. His value of 4.2×10^{19} erg/s should be reduced to 2.9×10^{19} erg/s.

PHILOSOPHICAL TRANSACTIONS OF THE ROYAL SOCIETY A MATHEMATICAL, PHYSICAL & ENGINEERING SCIENCES

At the boundaries $x = 0$ and $x = S$ we must satisfy the conditions of the continuity of ζ and of the tidal velocity u. The continuity of u requires that $\partial\zeta/\partial x$ be continuous, since

$$\frac{\partial u}{\partial t} = -g\frac{\partial \zeta}{\partial x} = \mathrm{i}\sigma u. \tag{A 12}$$

Using the relations
$$\frac{\partial \zeta}{\partial x} = -\frac{\sigma}{(gH)^{\frac{1}{2}}}\frac{\partial \zeta}{\partial y}, \quad \frac{\mathrm{d}}{\mathrm{d}y}J_0(y) = -J_1(y), \tag{A 13}$$

we are led to the equations
$$1 + R = AJ_0(y) + BY_0(y), \tag{A 14}$$

$$1 - R = \mathrm{i}AJ_1(y) + \mathrm{i}BY_1(y), \tag{A 15}$$

$$D\mathrm{e}^{-\mathrm{i}k'S} = AJ_0(y') + BY_0(y'), \tag{A 16}$$

$$D\mathrm{e}^{-\mathrm{i}k'S} = \mathrm{i}AJ_1(y') + \mathrm{i}BY_1(y'). \tag{A 17}$$

Putting
$$F(y) = J_0(y) - \mathrm{i}J_1(y), \quad G(y) = Y_0(y) - \mathrm{i}Y_1(y), \tag{A 18}$$

we get from (A 14)–(A 17)
$$A = 2G(y')/E, \tag{A 19}$$

$$B = -2F(y')/E, \tag{A 20}$$

$$R = [F(y)\,G(y') - G(y)\,F(y')]/E \tag{A 21}$$

$$D\mathrm{e}^{-\mathrm{i}k'S} = 4\mathrm{i}/(\pi y' E), \tag{A 22}$$

where
$$E = [F^*(y)\,G(y') - G^*(y)\,F(y')], \tag{A 23}$$

and the star denotes complex conjugate. In deriving (A 22), use was made of the relation

$$Y_0(y)\,J_1(y) - J_0(y)\,Y_1(y) = 2/(\pi y). \tag{A 24}$$

In applying the above sloping-shelf model to the real oceans we took for h the observed value of the ocean depth closest to the grid-point on the coast; S was taken as 100 km and h' was set equal to 10 m. At $x = 0$ in figure 3 we have

$$\zeta(0) = \sqrt{(h/g)}\left(\frac{1+R}{1-R}\right)u(0), \tag{A 25}$$

and this was the boundary condition applied in the computations at the grid points on the coast.

The kinetic energy crossing the point $x = S$, per unit time and per unit width of the coast, is

$$\mathrm{d}E'_k/\mathrm{d}t = -\tfrac{1}{2}\rho h' c' \langle u(S)^2\rangle = -\tfrac{1}{4}\rho |u(S)|^2 h'\sqrt{(gh')} = -\tfrac{1}{4}\rho g\sqrt{(gh')}\,DD^*. \tag{A 26}$$

This result follows first from the fact that, with the usual convention that an equation such as (A 3) means that ζ is equal to the real part of the right hand side, the time average $\langle u(S)^2\rangle$ is equal to $\frac{1}{2}|u(S)|^2$; and second from the relation

$$u(S) = \sqrt{(g/h')}\,D\mathrm{e}^{-\mathrm{i}k'S} = \sqrt{(g/h')}\,\zeta(S). \tag{A 27}$$

Since the potential energy is equal to the kinetic energy, the rate of dissipation of total energy per unit width of the coast is

$$\mathrm{d}E'/\mathrm{d}t = -\tfrac{1}{2}\rho g\sqrt{(gh')}\,DD^*. \tag{A 28}$$

The result (A 28) can also be derived as follows. We have for the change in pressure due to the tide

$$\delta p = g\rho\zeta. \tag{A 29}$$

Hence
$$\mathrm{d}E'/\mathrm{d}t = -h'\langle\delta p(S)\,u(S)\rangle = -g\rho h'\langle\zeta(S)\,u(S)\rangle$$
$$= -g\rho h'(h'/g)^{\frac{1}{2}}\langle u(S)^2\rangle = -\tfrac{1}{2}\rho g\sqrt{(gh')}\,DD^*. \quad \text{(A 30)}$$

In the above model, the amplitude ζ at $x = 0$ was normalized to equal $(1+R)$. For the actual computed tide ζ_c, the rate of dissipation of tidal energy per unit width of the coast is therefore

$$\frac{\mathrm{d}E}{\mathrm{d}t} = -\tfrac{1}{2}\rho g\sqrt{(gh')}\,DD^*|\zeta_c/(1+R)|^2. \quad \text{(A 31)}$$

We note from (A 21) and (A 22) the identity

$$c = cRR^* + c'DD^*, \quad \text{(A 32)}$$

where c denotes the velocity of propagation of the wave

$$c = \sqrt{(gh)}, \quad c' = \sqrt{(gh')}. \quad \text{(A 33)}$$

It can be shown that equation (A 32) expresses the equality of the incident wave-energy per unit time to the sum of the reflected and transmitted energies.

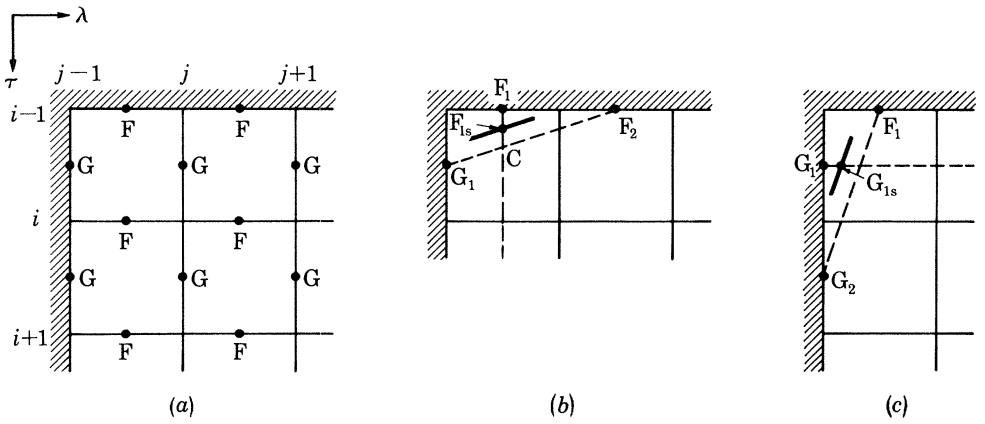

FIGURE 19. Numerical scheme and transition from rough coastline to smooth coastline.

APPENDIX B. REMARKS ON THE NUMERICAL SOLUTION

The southward and eastward components of the tidal velocity u and v were substituted by the functions F and G defined by (I, eqn (10))

$$hu = \frac{a}{\sin\theta}\frac{\partial F}{\partial t}, \quad hv = a\sin\theta\frac{\partial G}{\partial t}. \quad \text{(B 1)}$$

This substitution avoids the explicit differentiation of the depth $h(\theta, \lambda)$.

The system of differential equations for the functions F and G was approximated by finite differences in the (τ, λ) Mercator coordinate system, by using the well-known scheme of interlacing nets. The function F was defined on points of type $(i, j+\frac{1}{2})$ and the function G on points of type $(i+\frac{1}{2}, j)$ (figure 19*a*). In the rough-coastline model, the boundary was defined by arcs of latitude and longitude, and u_n, the velocity normal to the coast, was represented either through F or G at the boundary points.

The transition to a smooth-coastline model involves a shift of the points where the boundary condition is satisfied, as well as a change in the direction of the coastline.

Let F_1 be a boundary point on the rough coastline, G_1 and F_2 its immediate neighbours on the coastline (figure 19*b*). The line joining G_1 and F_2 intersects the longitude of F_1 at the point C. The boundary point for the smooth coastline-model will be shifted from F_1 to the point F_{1s} halfway between F_1 and C, with the direction of the coast parallel to the line $G_1 F_2$. The velocity normal to the coast is computed for the direction normal to the smoothed coastline at the point F_{1s}. The same procedure applies to boundary points of G type, where the latitude of the point G_{1s} is that of G_1 (figure 19*c*).

PHILOSOPHICAL TRANSACTIONS OF THE ROYAL SOCIETY A MATHEMATICAL, PHYSICAL & ENGINEERING SCIENCES

Appendix C. Love numbers h, k, l and loading Love numbers h', k', l'

Love numbers and loading Love numbers were computed for the Gutenberg model (Alterman *et al.* 1961) and for the continental model of Dziewonski *et al.* (1975). Up to the spherical harmonic order $n = 18$, the integration was carried out outwards from the centre towards the surface. For $n > 18$, the integrations were carried out from the surface inwards. These Love numbers were computed for the lunar semidiurnal tide for a period of 12.42 h. They were also used for the S_2 tide, since the dependence on period is small.

	Gutenberg model			Dziewonski *et al.* continental model		
n	h	k	l	h	k	l
2	0.6151	0.3035	0.0829	0.6126	0.3024	0.0849
3	0.2906	0.0934	0.0142	0.2921	0.0932	0.0148
4	0.1756	0.0420	0.0101	0.1773	0.0419	0.0102
5	0.1291	0.0247	0.0085	0.1304	0.0246	0.0085
6	0.1071	0.0170	0.0068	0.1081	0.0170	0.0068
7	0.0947	0.0129	0.0054	0.0955	0.0128	0.0054
8	0.0866	0.0102	0.0043	0.0873	0.0102	0.0043
9	0.0807	0.0084	0.0035	0.0813	0.0084	0.0035
10	0.0761	0.0071	0.0029	0.0767	0.0071	0 0028
11	0 0723	0.0061	0.0024	0.0729	0.0061	0.0024
12	0.0691	0.0053	0.0020	0.0697	0.0053	0.0020
13	0.0664	0.0047	0.0017	0.0669	0.0047	0.0017
14	0.0639	0.0042	0.0015	0.0646	0.0042	0.0014
15	0.0618	0.0038	0.0013	0.0626	0.0037	0.0012

	Gutenberg model			Dziewonski *et al.* continental model		
n	$-h'$	$-k'$	l'	$-h'$	$-k'$	l'
1	0.2859	0.0	0.1168	0.2907	0.0	0.1048
2	1.0125	0.3116	0.0298	1.0100	0.3102	0.0242
3	1.0607	0.1972	0.0750	1.0723	0.1989	0.0724
4	1.0598	0.1336	0.0622	1.0768	0.1353	0.0614
5	1.0932	0.1044	0.0490	1.1120	0.1058	0.0489
6	1.1524	0.0901	0.0412	1.1725	0.0911	0.0414
7	1.2228	0.0819	0.0367	1.2446	0.0827	0.0371
8	1.2960	0.0764	0.0338	1.3199	0.0771	0.0345
9	1.3683	0.0723	0.0318	1.3947	0.0729	0.0328
10	1.4383	0.0690	0.0304	1.4673	0.0695	0.0316
11	1.5053	0.0662	0.0292	1.5372	0.0667	0.0307
12	1.5695	0.0638	0.0283	1.6043	0.0643	0.0300
13	1.6308	0.0616	0.0275	1.6685	0.0621	0.0294
14	1.6894	0.0598	0.0269	1.7300	0.0602	0.0289
15	1.7455	0.0580	0.0264	1.7888	0.0584	0.0286
16	1.7991	0.0564	0.0259			
17	1.8500	0.0549	0.0255			
18	1.9002	0.0535	0.0251			
19	1.9462	0.0522	0.0248			
20	1.9909	0.0509	0.0244			
21	2.0336	0.0498	0.0242			
22	2.0743	0.0486	0.0239			
23	2.1132	0.0475	0.0236			
24	2.1503	0.0465	0.0233			
25	2.1857	0.0455	0.0230			
26	2.2194	0.0445	0.0228			
27	2.2517	0.0435	0.0225			
28	2.2824	0.0426	0.0223			
29	2.3118	0.0417	0.0220			
30	2.3399	0.0409	0.0217			

References

Alterman, Z., Jarosch, H. & Pekeris, C. L. 1961 *Geophys. J. R. astr. Soc.* **4**, 219–241.
Bogdanov, K. T. & Magarik, V. 1967 *Dokl. Akad. Nauk. SSSR* **172**, 1315–1317.
Cartwright, D. E. 1971 *Phil. Trans. R. Soc. Lond.* A **270**, 603–649.
Dietrich, G. 1944 *Veröffentl. Inst. Meereskunde Univ. Berlin* A **41**, 7–68.
Dishon, M. & Heezen, B. C. 1968 *Int. Hydrographic Rev.* **45**, 23–39.
Dziewonski, A. M., Hales, A. L. & Lapwood, E. R. 1975 *Phys. Earth Planet. Inter.* **10**, 12–48.
Farrell, W. E. 1972 *Nature, Lond.* **238**, 43–44.
Farrell, W. E. 1973 *Phil. Trans. R. Soc. Lond.* A **274**, 253–259.
Gordeev, R. G., Kagan, B. A. & Polyakov, E. V. 1977 *J. Phys. Oceanog.* **7**, 161–170.
Harrison, J. C., Ness, N. F., Longman, I. M., Forbes, R. F. S., Kraut, E. A. & Slichter, L. B. 1963 *J. Geophys. Res.* **68**, 1497–1516.
Hendershott, M. & Munk, W. 1970 *A. Rev. Fluid Mech.* **2**, 205–244.
Hendershott, M. C. 1972 *Geophys. J. R. astr. Soc.* **29**, 389–402.
Irish, J., Munk, W. & Snodgrass, F. 1971 *Geophys. Fluid Dynamics* **2**, 355–360.
Jeffreys, H. 1968 *Geophys. J. R. astr. Soc.* **16**, 253–258.
Jeffreys, H. 1970 *The Earth*, 5th edn, p. 314, Cambridge University Press.
Jeffreys, H. 1975 *Q. J. astr. Soc.* **16**, 150.
Jeffreys, H. 1976 *The earth*, 6th edn, Cambridge University Press.
Kuo, J. T. & Jachens, R. C. 1977 *Annls. Géophys.* **33**, 73–82.
Lamb, H. 1932 *Hydrodynamics*. Cambridge University Press.
Lambeck, K. 1977 *Phil. Trans. R. Soc. Lond.* A **287**, 543–594.
Laplace, P. S. 1775 *Mem. math. phys. Acad roy. Soc., Paris*, pp. 75–182.
Larsen, J. C. 1977 *J. Phys. Oceanogr.* **7**, 100–109.
Pekeris, C. L. & Accad, Y. 1969 *Phil. Trans. R. Soc. Lond.* A **265**, 413–436.
Pekeris, C. L. & Accad, Y. 1972 *Phil. Trans. R. Soc. Lond.* A **273**, 237–260.
Proudman, J. 1941 *Mon. not. R. astr. Soc., Geophys. Sec.* **5**, 23–26.
Tiron, K. D., Sergeev, Y. & Michurin, A. 1967 *Vestn. Leningrad Univ.* **24**, 123–145.

PHILOSOPHICAL TRANSACTIONS OF THE ROYAL SOCIETY A MATHEMATICAL, PHYSICAL & ENGINEERING SCIENCES